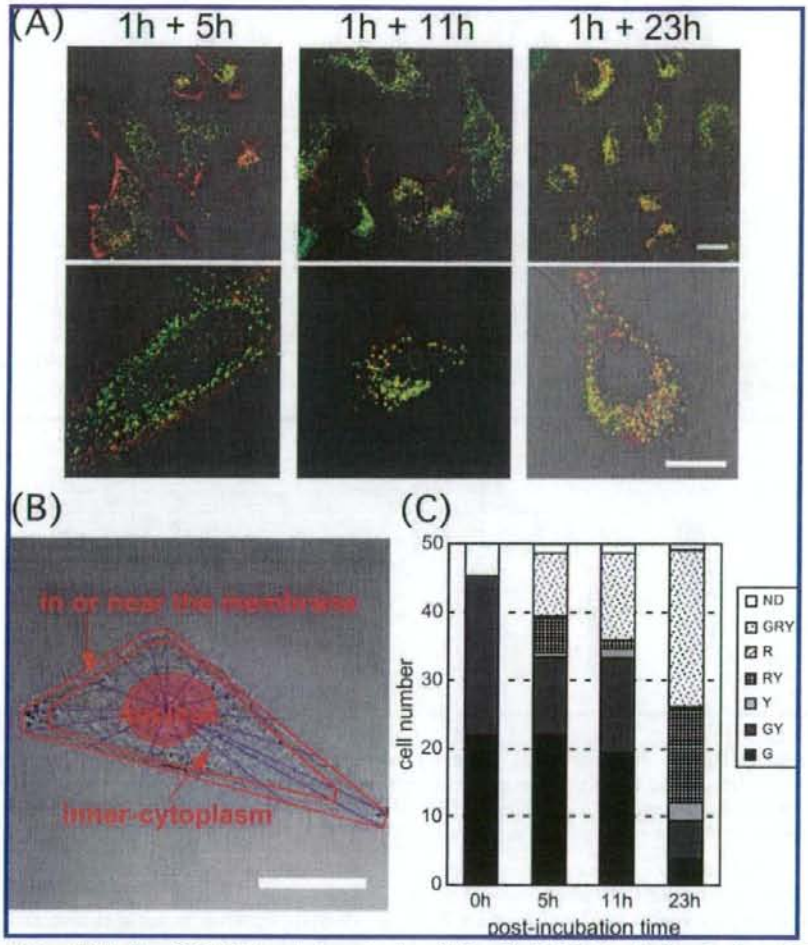


***Figure 4.*** Intracellular distribution B-SH11% polyplex micelles (N/P = 2). RGD (−) micelles loading Cy5-labeled pDNA (red) and RGD (+) micelles loading Cy3-labeled pDNA (green) were simultaneously added and incubated with HeLa cells for 1 h. After replacement with fresh medium, cells were reincubated for the indicated reincubation times (5 h, 11 h, 23 h). (A) CLSM images. Scale bars represent 20 $\mu$m. (B) Definitions of "nucleus", "inner-cytoplasm", and "in or near the membrane" regions. "Inner-cytoplasm" was defined as three-quarters of the area from the nucleus to the cell membrane, and "in or near the membrane" was defined as the remaining quarter on the side of the cell membrane. (C) Quantitative analysis of the inner-cytoplasmic distribution of pDNA transfected by polyplex micelles with or without RGD ligands. Fifty different cells were observed and evaluated for each time point. G: green (Cy3-labeled pDNA loaded in RGD (+) micelles). R: red (Cy5-labeled pDNA loaded in RGD (−) micelles). Y: yellow (colocalized Cy3-labeled and Cy5-labeled pDNAs). ND: not detectable (no colors detectable from pDNA).

(Perkin-Elmer, Waltham, MA). Measurements were performed using the Tricarb 2200CA liquid scintillation analyzer (Packard, Meriden, CT) with a counting time of 1 min. The amounts of uptaken pDNA were calculated using a standard curve calibrated with naked $^{32}$P-labeled pDNA.

**CLSM Observation.** pDNA was labeled with Cy3 or Cy5 according to the manufacturer's protocol. Briefly, pDNA was labeled using the Label IT Nucleic Acid Labeling Kit (Mirus, Madison, WI). HeLa cells (30 000 cells) were seeded on a 35 mm glass base dish (Iwaki, Tokyo, Japan) and incubated overnight in 1 mL of DMEM containing 10% FBS, followed by replacement with fresh medium. In the simultaneous observation of RGD (−) and RGD (+) micelles (Figure 4), RGD (−) B-SH11% polyplex micelle solution containing 3 $\mu$g Cy5-labeled pDNA (N/P = 2) and RGD (+) B-SH11% polyplex micelle solution containing 3 $\mu$g Cy3-labeled pDNA (N/P = 2) were simultaneously applied to a glass dish with cultured HeLa cells. The measurement condition was adjusted so as to obtain almost the same fluorescence intensities between RGD (+) B-SH11% micelles containing Cy3-

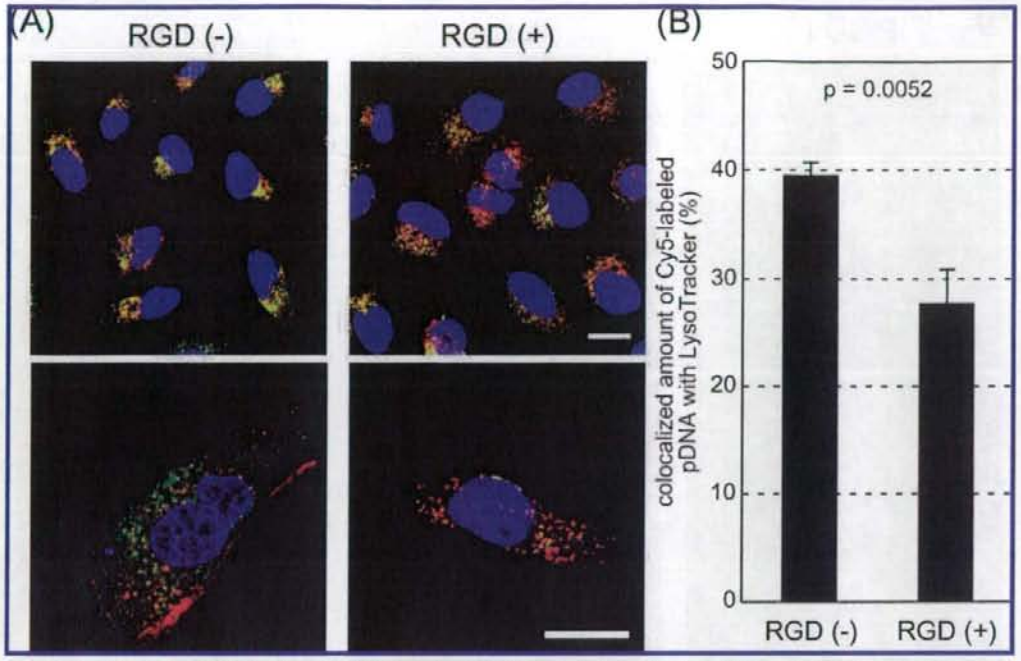


***Figure 5.*** Distribution of RGD (+) and RGD (−) B-SH11% polyplex micelles (N/P = 2) in late endosomes and lysosomes. Polyplex micelles loading Cy5-labeled pDNA (red) were incubated with HeLa cells for 1 h. After replacement with fresh medium, the cells were reincubated for 11 h. The cell nuclei were stained with Hoechst 33342 (blue), and the acidic late endosomes and lysosomes were stained with LysoTracker Green (green). (A) CLSM images of the cells transfected with RGD (−) micelles (left) and RGD (+) micelles (right). The scale bars represent 20 $\mu$m. (B) Quantification of Cy5-labeled pDNA colocalized with LysoTracker Green in the inner-cytoplasm. Error bars in the graph represent SEM ($n$ = 10).

labeled pDNA and RGD (+) B-SH11% micelles containing Cy5-labeled pDNA. In the observation with organelle staining (Figures 5 and 6), either RGD (−) or RGD (+) B-SH11% polyplex micelle solution containing Cy5-labeled pDNA (N/P = 2) was applied to a dish with cultured HeLa cells. After various incubation periods, the medium was removed and the cells were washed 3 times with PBS. The intracellular distribution of the polyplex micelles was observed by CLSM after staining acidic late endosomes and lysosomes with LysoTracker Green (Molecular Probes, Eugene, OR), lipid rafts and caveosomes with cholera toxin subunit B (CT-B) Alexa Fluor 488 conjugate (Molecular Probes), and the nuclei with Hoechst 33342 (Dojindo Laboratories, Kumamoto, Japan). The CLSM observation was performed using an LSM 510 (Carl Zeiss, Oberlochen, Germany) with a C-Apochromat 63X objective (Carl Zeiss) at the excitation wavelength of 488 nm (Ar laser) for LysoTracker Green and CT-B Alexa Fluor 488, 543 nm (He−Ne laser) for Cy3, 633 nm (He−Ne laser) for Cy5, and 710 nm (MaiTai laser, two photon excitation; Spectra-Physics, Mountain View, CA) for Hoechst 33342, respectively.

**Evaluation of Intracellular Distribution of Polyplex Micelles.** To evaluate the amounts of polyplex micelles in cytoplasm, polyplex micelles internalized into the inner region of the cytoplasm were distinguished from polyplex micelles adsorbing onto the cell membrane by reference to a previous paper,[16] in which the cytoplasm was divided into four quadrants to study the intracellular spatial variation of polyplexes (Figure 4B). First, an intracellular region was divided into three areas: "nucleus", "inner-cytoplasm", and "in or near the membrane". "Inner-cytoplasm" was defined as a three-quarters of the area from the nucleus to the cell membrane, and "in or near the membrane" was defined as remaining quarter area on the side of the cell membrane, as illustrated in Figure 4B. From the observation of 50 different cells, the relative amounts of RGD (−) micelles (red) and RGD (+) micelles (green) in the "inner-cytoplasm" were determined based on the number of cells. The following abbreviations are used in Figure 4C: G, green (Cy3-labeled pDNA); R, red (Cy5-labeled pDNA); Y, yellow (Cy3-labeled pDNA colocalized with Cy5-labeled pDNA); and ND, not detectable (no colors (pDNA) detectable). In brief, GRY represents cells with green, red, and yellow spots indepen-

(16) Suh, J.; Wirtz, D.; Hanes, J. Efficient Active Transport of Gene Nanocarriers to the Cell Nucleus. *Proc. Natl. Acad. Sci. U.S.A.* **2003**, *100*, 3878–3882.

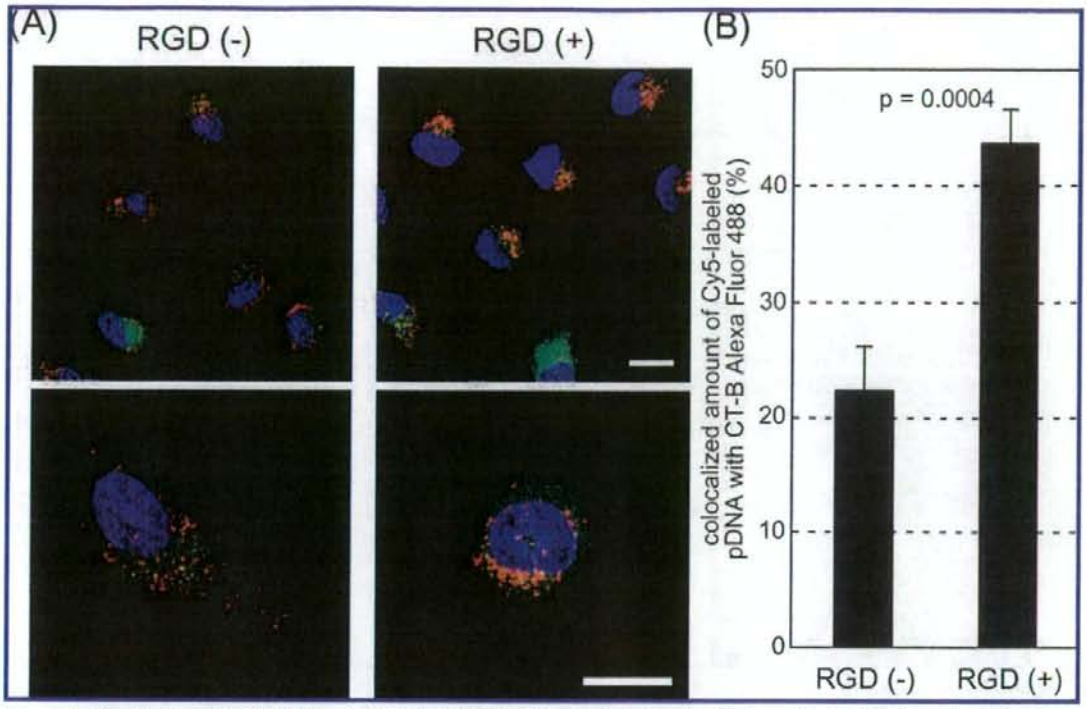


***Figure 6.*** Distribution of RGD (+) and RGD (−) B-SH11% polyplex micelles (N/P = 2) in lipid rafts and caveosomes. Polyplex micelles loading Cy5-labeled pDNA (red) and CT-B Alexa Fluor 488 conjugate (green) were incubated with HeLa cells for 1 h. After replacement with fresh medium, the cells were reincubated for 11 h. The cell nuclei were stained with Hoechst 33342 (blue). (A) CLSM images of RGD (−) micelles (left) and RGD (+) micelles (right). The scale bars represent 20 $\mu$m. (B) Quantification of Cy5-labeled pDNA colocalized with CT-B in the inner-cytoplasm. Error bars in the graph represent SEM ($n$ = 10).

dently existing in the "inner-cytoplasm", and GY represents cells with green and yellow spots but without red spots.

To evaluate the final destinations of polyplex micelles, the rate of colocalization of Cy5-labeled pDNA with LysoTracker Green or CT-B Alexa Fluor 488 was quantified (Figures 5B and 6B). LysoTracker Green was used as a marker for the late endosomes and the lysosomes, and CT-B Alexa Fluor 488 was used as a marker for the lipid rafts and the caveosomes. Colocalization was quantified as follows:

$$\text{amount of colocalization (\%)} = \text{Cy5 pixels}_{\text{colocalization}}/\text{Cy5 pixels}_{\text{total}} \times 100$$

where Cy5 $\text{pixels}_{\text{colocalization}}$ represents the number of Cy5 pixels colocalizing with LysoTracker Green or CT-B Alexa Fluor 488 in the inner-cytoplasm, and Cy5 $\text{pixels}_{\text{total}}$ represents the number of all Cy5 pixels in the inner-cytoplasm.

**Real-Time Luciferase Gene Expression.** HeLa cells (40 000 cells) were seeded on a 35 mm dish (Becton Dickinson, Franklin Lakes, NJ) and incubated overnight in 2 mL of DMEM containing 10% FBS, with or without 10 $\mu$g/mL aphidicolin for synchronization of cells. The HeLa cell cycle was arrested in a phase between G1 and S by over 16 h incubation with aphidicolin.[17] The subsequent replacement with fresh medium let cells start to divide at 13 h later. In this assay, three experimental conditions were used to regulate the lag between the time the polyplex micelles were added and the beginning of mitosis. First was the "normal" condition, meaning without any treatments for synchronization. Second was the "3 h mitosis" condition, where each polyplex micelle was added 10 h after the replacement of medium containing aphidicolin with fresh medium, thus setting the start of cell mitosis 3 h after the addition of polyplex micelles. Third was the "13 h mitosis" condition, where each polyplex micelle was added just after the medium replacement, thus commencing cell mitosis 13 h after the addition of the micelles. In the case of the "normal" and "13 h mitosis" conditions, after replacement with fresh medium containing 0.1 mM D-luciferin, RGD (−) or RGD (+) B-SH11% polyplex micelles (N/P = 2) containing 3 $\mu$g of pDNA were immediately added. In the case of the "3 h

(17) Pedrali-Noy, G.; Spadari, S.; Miller-Faures, A.; Miller, A. O. A.; Kruppa, J.; Koch, G. Synchronization of HeLa Cell Cultures by Inhibition of DNA Polymerase α with Aphidicolin. *Nucleic Acids Res.* **1980**, *8*, 377–387.

mitosis" condition, polyplex micelles were added 10 h after the replacement with fresh medium containing 0.1 mM D-luciferin. The dishes were set in a luminometer incorporated in a $CO_2$ incubator (AB-2550 Kronos Dio, ATTO, Tokyo, Japan), and the bioluminescence was monitored every 20 min with an exposure time of 2 min.

## Results

**Synthesis of c(RGDfK)-PEG-P(Lys-MP).** (Scheme 1). Thiolation of acetal-PEG-PLys block copolymer was carried out using a previously described method.[9] Briefly, SPDP was used as a thiolating reagent and reacted with $\varepsilon$-amino group of Lys unit; consequently, a 3-(2-pyridyldithio)propionyl (PDP) group was introduced via an amide bond. Note that the introduction of the thiol group by SPDP decreased the cationic charge density of the PLys segment as the introduction rate increased. Thiolated acetal-PEG-P(Lys-PDP) block copolymers with two types of thiolation degree, 5.04% (B-SH5%) and 10.5% (B-SH11%), were prepared. The PDP introduction rates were calculated from the peak intensity ratio of the methylene protons of PEG ($OCH_2CH_2$, $\delta = 3.7$ ppm) to the pyridyl protons of the PDP group ($C_5H_4N$, $\delta =$ 7.0−8.5 ppm) measured by $^1$H NMR as typically seen in Figure 1B (B-SH5%).

Conjugation of c(RGDfK) peptide ligands into the PEG terminus of acetal-PEG-P(Lys-PDP) was achieved through the formation of a thiazolidine ring between an N-terminal cysteine and an aldehyde group converted from the acetal group.[11] The acetal group was deprotected under moderate acidic conditions to the aldehyde group. To avoid an exchange reaction between the thiol group of cysteine residue in the c(RGDfK) peptide and the pyridylthio group in the acetal-PEG-P(Lys-PDP), the pyridylthio group was deprotected with DTT prior to the installation of the ligand. After the dialysis against the AcOH buffer to remove excessive DTT as well as to convert the acetal group to an aldehyde group, the c(RGDfK) peptide was added to react with the aldehyde-PEG-P(Lys-MP) in AcOH buffer, resulting in the introduction of the peptide ligand. This type of conjugation between the N-terminal cysteine and the aldehyde group occurs selectively even in the presence of primary amines, since the conjugation through a Schiff base between a primary amine and the aldehyde group is reversible, whereas the conjugation through a thiazolidine ring between the N-terminal cysteine and the aldehyde group is irreversible. The methyl protons of the acetal group ($\delta = 1.2$ ppm) and the aromatic protons of the pyridylthio group ($\delta = 7.0-8.5$ ppm) completely disappeared with the appearance of protons assigned to the aromatic ring of D-phenylalanine (f: D-Phe) ($\delta = 7.3$ and 7.4 ppm) in the c(RGDfK) (Figure 1C). Based on the peak intensity ratios of the aromatic protons of the peptide ligands to the methylene protons of PEG ($\delta = 3.7$ ppm), the introduction rates of the peptide ligands in the c(RGDfK)-PEG-P(Lys-MP) were determined to be 73% and 87% for the B-SH5% and the B-SH11%, respectively.

**Formation of Polyplex Micelles.** Agarose gel electrophoresis showed that free pDNA was not detected in the polyplex micelles at N/P = 2 (data not shown), confirming that all of the pDNA were entrapped in polyplex micelles. Ellman's test revealed that less than 2% of the thiol groups in the polyplex micelles were free (data not shown), suggesting that almost all of the thiol groups seem to be involved in the formation of disulfide bonds. These results are consistent with our previous report.[9] The sizes, shapes, and $\zeta$-potentials of the cross-linked polyplex micelles were evaluated by DLS, AFM, and laser-doppler electrophoresis, respectively. Table 1 summarizes the cumulant diameters and $\zeta$-potentials of the polyplex micelles at N/P = 2. The cumulant diameters of all the micelles were approximately 110 nm with a moderate polydispersity index between 0.14 and 0.18, regardless of the composition of the thiolated polymers or the introduction of RGD ligands. Also, the $\zeta$-potentials of all the micelles were kept at slightly positive values between +1.1 and +3.6, which is consistent with the formation of the PEG palisade surrounding the polyplex core.[6,18] Figure 2 shows AFM images of B-SH11% cross-linked micelles with or without RGD ligands, where a toroidal structure in the size range of 60−100 nm and a rodlike structure with a long axis of 160−200 nm were observed, corresponding to the sizes from DLS. These results suggest that the physicochemical characteristics of the polyplex micelles are quite similar regardless of the thiolation degree or the introduction of RGD ligands.

***Table 1.*** Size and $\zeta$-Potential of Polyplex Micelles (N/P = 2) with or without Cyclic RGD Peptide Ligands

| thiolation degree (%) | cyclic RGD peptide ligand | cumulant diameter (nm)/ polydispersity index ($\mu/\Gamma^2$) | $\zeta$-potential (mV) |
|---|---|---|---|
| 0 | (−) | 109 ± 0.75/0.169 ± 0.002 | 1.47 ± 0.312 |
| | (+) | 113 ± 1.11/0.156 ± 0.004 | 2.27 ± 0.148 |
| 5 | (−) | 115 ± 0.71/0.141 ± 0.007 | 1.62 ± 0.348 |
| | (+) | 106 ± 0.48/0.144 ± 0.009 | 3.57 ± 0.230 |
| 11 | (−) | 111 ± 0.25/0.145 ± 0.011 | 1.15 ± 0.788 |
| | (+) | 114 ± 1.08/0.172 ± 0.005 | 1.52 ± 0.213 |

**Transfection.** The *in vitro* transfection efficiencies of B-SH0%, B-SH5%, and B-SH11% polyplex micelles with or without RGD ligands were evaluated for HeLa cells possessing $\alpha_v\beta_3$ and $\alpha_v\beta_5$ integrin receptors (Figure 3A). A cyclic RGD peptide is well-known to selectively recognize $\alpha_v\beta_3$ and $\alpha_v\beta_5$ integrins among several integrins.[19] In the transfection experiments with non-cross-linked micelles (B-SH0% micelle), the introduction of RGD ligands led to approximately doubled transfection efficiency. Notably, RGD (+) B-SH5% and RGD (+) B-SH11% micelles with cross-

(18) Harada-Shiba, M.; Yamauchi, K.; Harada, A.; Takamisawa, I.; Shimokado, K.; Kataoka, K. Polyion Complex Micelles as Vectors in Gene Therapy-Pharmacokinetics and In Vivo Gene Transfer. *Gene Ther.* **2002**, *9*, 407–414.

(19) Haubner, R.; Gratias, R.; Difenbach, B.; Goodman, S. L.; Jonczyk, A.; Kessler, H. Structual and Functional Aspects of RGD-Containing Cyclic Pentapeptides as Highly Potent and Selective Integrin $\alpha_v\beta_3$ Antagonists. *J. Am. Chem. Soc.* **1996**, *118*, 7461–7472.

linked cores and RGD ligands showed 10-fold higher efficiency than the ligand-less system without cross-linking (RGD (−) B-SH0% micelle). It is obvious that the effect of ligand installation was drastically enhanced by introducing disulfide cross-linking in the core. RGD (+) B-SH5% polyplex micelles achieved the highest transfection efficiency. Consequently, the combination of core cross-linking and ligand installation enhanced efficiency 20 times more than the polyplex micelles without ligands and cross-links.

Then, to further confirm that the increased transfection efficiency by RGD (+) micelles involves the receptor-mediated mechanism, a competitive assay using free cyclic RGD peptides was carried out for B-SH11% cross-linked micelles (Figure 3B). RGD (+) micelles showed a remarkably high transfection efficiency compared with RGD (−) micelles in the absence of free cyclic RGD peptides ($P < 0.01$). As the concentration of free cyclic RGD peptides increased, the transfection efficiency of RGD (+) micelles accordingly decreased, approaching the transfection level of RGD (−) micelles under the condition of 100 $\mu$M cyclic RGD peptides ($P = 0.104$). Thus, the results of the competitive assay indicate that $\alpha_v\beta_3$ and/or $\alpha_v\beta_5$ integrin receptor-mediated endocytosis is involved in the transfection of the RGD (+) micelles against HeLa cells.

**Analysis of Cellular Uptake of Polyplex Micelles.** In general, the enhanced transfection by ligands has been attributed to an increased uptake of vectors.[14,20,21] Thus, the cellular uptake of the RGD (−) and RGD (+) micelles into the HeLa cells was evaluated using a system loaded with $^{32}$P-labeled pDNA (Figure 3C). Regardless of ligand installation, cross-linked micelles tend to be taken up more efficiently than noncrosslinked micelles. The introduction of disulfide cross-links into the micelle core appreciably contributes to an increase in the stability of micelles under physiological conditions.[9] This implies that disulfide cross-links might prevent the micelles from dissociation in the extracellular medium, and consequently facilitate their internalization into the cellular compartment. Interestingly, there is no significant increase in micelle uptake even by installing RGD ligands, suggesting that other factors, including modulation of intracellular trafficking, may be involved in the enhancement of transfection efficiency by cyclic RGD peptide ligands.

**Intracellular Distribution of Polyplex Micelles.** Our previous report showed that RGD (+) polyplex micelles preferentially localize in the perinuclear region, unlike RGD (−) polyplex micelles,[11] suggesting that RGD ligands likely modulate intracellular trafficking of polyplex micelles. Therefore, detailed observation of the intracellular distribution was carried out using CLSM (Figure 4). The medium was replaced with fresh medium after 1 h incubation of polyplex micelles with cultured HeLa cells. Then CLSM observation was carried out after each reincubation without polyplex micelles in the medium. The CLSM images are shown in Figure 4A. The micelles localized in the inner-cytoplasm were quantitatively evaluated using the procedure described in the Experimental Section and shown in Figure 4B; the data are summarized in Figure 4C. After the 5 h reincubation (total 6 h incubation), the spots observed in the inner region of the cytoplasm were mainly the green spots of RGD (+) micelles (Figure 4A, left). On the other hand, the RGD (−) micelles, shown in red stayed mainly near the cell membrane (Figure 4A, left), but some fraction was observed in the inner-cytoplasm as red spots (RGD (−) micelle alone) or yellow spots (colocalizing with RGD (+) micelles). In the early stages, almost half of the cell population with fluorescence had only green spots, corresponding to the internalization of RGD (+) micelles (Figure 4C); this indicated that RGD (+) micelles were internalized into the inner-cytoplasm much faster than RGD (−) micelles. However, further reincubation resulted in the decrease in the cell fraction that showed only green spots and lead to an increase in the fraction that included yellow spots, corresponding to the colocalization of RGD (−) and RGD (+) micelles, as well as to an increase in red spots, corresponding to the presence of RGD (−) micelles alone. Note that there are two possibilities for the appearance of yellow spots. The first is that RGD (−) and RGD (+) micelles adsorbing to the cell membrane were simultaneously endocytosed by the cell. The second is that RGD (−) and RGD (+) micelles that were separately internalized into the cells subsequently colocalized through the possible fusion of the compartments in the inner-cytoplasm. On the other hand, the green spots still existed in a definite fraction of cells (G + GY + GRY) even after long-term reincubation, while the fraction of the cells including red spots (R + RY + GRY) continued to increase (Figure 4C). Thus, it is reasonable to assume that there may be distinct routes of internalization for RGD (−) and RGD (+) micelles, and eventually their final destinations may be different.

To examine whether or not RGD ligand installation in the micelles alters their intracellular trafficking, organelles were selectively stained using LysoTracker for the late endosomes and the lysosomes, and CT-B for the lipid rafts and the caveosomes (Figures 5 and 6).[22,23] In this experiment, the medium was replaced 1 h after the addition of polyplex micelles, followed by 11 h of reincubation. The rate of colocalization was quantified by the formula shown in the Experimental Section. The experiment with LysoTracker revealed that 39% of RGD (−) micelles and 28% of RGD (+) micelles in the inner-cytoplasm were localized in the late endosomes and lysosomes, indicating that the colocalization ratio of RGD (−) micelles with the late endosomes and lysosomes was significantly higher than that of RGD (+) micelles ($P = 0.0052$) (Figure 5B). On the other hand, the observation with CT-B revealed that 22% of RGD (−)

(20) de Bruin, K.; Ruthardt, N.; von Gersdorff, K.; Bausinger, R.; Wagner, E.; Ogris, M.; Bräuchle, C. Cellular Dynamics of EGF Receptor-Targeted Synthetic Viruses. *Mol. Ther.* **2007**, *15*, 1297–1305.

(21) Vinogradov, S.; Batrakova, E.; Li, S.; Kabanov, A. Polyion Complex Micelles with Protein-Modified Corona for Receptor-Mediated Delivery of Oligonucleotides into Cells. *Bioconjugate Chem.* **1999**, *10*, 851–860.

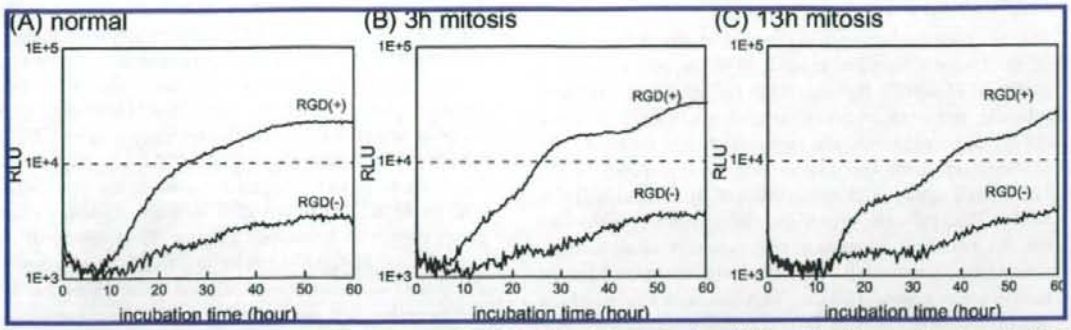


*Figure 7.* Real-time luciferase gene expression of B-SH11% polyplex micelles (N/P = 2) with or without cyclic RGD peptide ligands under the "normal" condition (A), the "3 h mitosis" condition (B), and the "13 h mitosis" condition (C).

micelles and 44% of RGD (+) micelles in the inner-cytoplasm were localized in the lipid rafts and caveosomes, respectively, indicating that the RGD (+) micelles had significantly higher localization ratios to the lipid rafts and caveosomes than the RGD (−) micelles ($P = 0.0004$) (Figure 6B). These results indicate that the polyplex micelles with cyclic RGD ligands were internalized preferentially through caveolae-mediated endocytosis by HeLa cells.

**Real Time Luciferase Gene Expression.** In the conventional luciferase assay, transfected cells need to be lysed before measurement, and this restricts the evaluation of luciferase expression in real time. Alternatively, as explained in the Experimental Section, Kronos Dio allows us to measure real-time luciferase expression while maintaining the cell culture for a prolonged period.[24] Figure 7 shows the results of time-dependent gene expression with RGD (−) and RGD (+) B-SH11% micelles. Under the "normal" condition without any control over the cell cycle (Figure 7A), the luciferase expression with RGD (−) and RGD (+) micelles started almost simultaneously around 8 h after the micelles were added. The expression of genes reached a plateau after around 50 h of incubation regardless of the presence of RGD ligands. Considering that the half-life of luciferase is about 2−3 h in living cells,[25] the rate of luciferase production is expected to be equal to that of luciferase degradation in regions over 50 h. RGD (+) micelles showed higher transfection rates than RGD (−) micelles at all time points. Real-time gene expression was assessed for cells after aphidicolin, a DNA synthesis inhibitor, was used to synchronize the cell cycle (Figures 7B and 7C). HeLa cells incubated with aphidicolin for more than 16 h are arrested between the G1 and S phases,[17] and a change to a medium that dose not contain aphidicolin allows HeLa cells to progress into the S phase to divide 13 h later. We confirmed that almost all HeLa cells were in the S phase immediately after the medium replacement and were in the G2 phase 10 h after the replacement (data not shown). Under the "3 h mitosis" condition, where cell division started 3 h after polyplex micelles were added (Figure 7B), gene expression by RGD (+) micelles was detected 5 h after incubation, while that of RGD (−) micelles was below the Kronos Dio detection limit even after about 12 h of incubation. This implies that RGD (+) micelles can migrate into the nucleus during the first mitosis due to their early accumulation in the perinuclear region, whereas this is not the case for RGD (−) micelles because of their slow accumulation in that region. Under the "13 h mitosis" condition, where cell division started 13 h after polyplex micelles were added (Figure 7C), luciferase expression with RGD (−) and RGD (+) micelles was detected simultaneously at 13 h after incubation, which corresponds to the initiation of cell division. This result suggests that RGD (+) micelles move early to the perinuclear region but may not be actively transported into the nucleus in the nonmitotic condition. As shown in Figure 4, most of the RGD (−) micelles were internalized into the cell to accumulate in the perinuclear region at a level comparable to that of RGD (+) micelles after 24 h of incubation. Nevertheless, RGD (−) micelles under the "13 h mitosis" condition exhibited remarkably lower increases in luciferase expression at more than 30 h of incubation compared to RGD (+) micelles. Apparently, this cannot be explained by the difference in the migration rate between RGD (−) and RGD (+) micelles because of their similar levels of accumulation in the perinuclear region in this time period. Presumably, this might be explained by the difference in the final destinations of the polyplex micelles with and without cyclic RGD ligands due to the modulation of intracellular trafficking as shown in Figures 5 and 6.

(22) Orlandi, P. A.; Fishman, P. H. Filipin-Dependent Inhibition of Cholera Toxin: Evidence for Toxin Internalization and Activation through Caveolae-Like Domains. *J. Cell Biol.* **1998**, *141*, 905–915.

(23) von Gersdorff, K.; Sanders, N. N.; Vandenbroucke, R.; de Smedt, S. C.; Wagner, E.; Ogris, M. The Internalization Route Resulting in Successful Gene Expression Depends on both Cell Line and Polyethylenimine Polyplex Type. *Mol. Ther.* **2006**, *14*, 745–753.

(24) Takae, S.; Miyata, K.; Oba, M.; Ishii, T.; Nishiyama, N.; Itaka, K.; Yamasaki, Y.; Koyama, H.; Kataoka, K. PEG-Detachable Polyplex Micelles Based on Disulfide-Linked Block Catiomers as Bioresponsive Nonviral Gene Vectors. *J. Am. Chem. Soc.* **2008**, *130*, 6001–6009.

(25) Ignowski, J. M.; Schaffer, D. V. Kinetic Analysis and Modeling of Firefly Luciferase as a Quantitative Reporter Gene in Live Mammalian Cells. *Biotechnol. Bioeng.* **2004**, *86*, 827–834.

## Discussion

In the present study, two distinctive implementations, that of environment-sensitive cross-links in the core and that of cyclic RGD peptide ligands on the surface, were integrated into the polyplex micelles formed by PEG-PLys block copolymers and pDNA. The physicochemical characteristics of these micelles were quite similar regardless of the thiolation degree or the introduction of RGD ligands (Table 1). The PEG palisade surrounding the polyplex core shielded the charges of the micelles to maintain very small absolute values in the $\zeta$-potentials. The cumulant diameter of polyplex micelles was around 100 nm. This indicates that all of the polyplex micelles possess favorable characteristics relevant to future *in vivo* application. In transfection experiments using cultured cells, polyplex micelles with cyclic RGD ligands achieved higher transfection efficiency than polyplex micelles without cyclic RGD ligands against HeLa cells appreciably expressing $\alpha_v\beta_3$ integrin receptors (Figure 3A). Interestingly, RGD ligands' effect on transfection was further enhanced by the introduction of disulfide cross-linking in the micelle core. Disulfide cross-links have been reported to stabilize polyplex micelles against the counter polyanion exchange reaction under nonreductive conditions.[9] Therefore, cross-linked micelles might acquire greater stability in the medium compared to noncrosslinked micelles, indicating the enhanced effect of cyclic RGD ligands. Note that RGD (+) B-SH5% micelles achieved the highest transfection efficiency among all micelles. Excessive cross-linking into the cores of polyplex micelles has been reported to overstabilize the micelles and impede the release of pDNA,[9] which is considered to be a cause of the lower transfection efficiency of B-SH11% micelles compared to that of B-SH5% micelles. The inhibitory experiment using free cyclic RGD peptides (Figure 3B) certainly confirmed that receptor-mediated uptake by RGD ligands contributed to the enhancement of gene expression. It is worth noting that the enhancement was not due to an increase in the cellular uptake of polyplex micelles (Figure 3C), suggesting that cyclic RGD peptide ligands may modulate the intracellular trafficking of the polyplex micelles, leading to increased transfection efficiency. In this regard it should be noted that, in our previous study, cyclic RGD ligands facilitated the transport of the polyplex micelles to the perinuclear region.[11] Other studies found that some ligands, such as b-FGF[26] and lactose,[27] contribute to the change in the intracellular trafficking of gene vectors. Time-dependent CLSM observation revealed that RGD (+) micelles were internalized into the cytoplasm and moved to the perinuclear region much earlier than RGD (−) micelles (Figure 4). This is consistent with the results of real-time luciferase expression under the "3 h mitosis" condition, where RGD (+) micelles exhibited earlier onset of gene expression with high efficiency (Figure 7B). The CLSM observation also clarified the variation in final localization in the cytoplasm between the two micelles (Figure 4). CLSM observation with the staining of acidic endosomes and lysosomes (Figure 5) or lipid rafts and caveosomes (Figure 6) revealed that RGD (+) micelles were distributed in the acidic organelles at lower levels than RGD (−) micelles, and were preferentially internalized via caveolae-mediated endocytosis. Considering that pDNA degradation occurs in late endosomes and lysosomes by enzymatic hydrolysis, RGD (+) micelles are more likely than RGD (−) micelles to protect entrapped pDNA from enzymatic degradation. It is known that cells uptake particles of different sizes through different routes: macropinocytosis (>200 nm), clathrin-mediated endocytosis (100−200 nm), and caveolae-mediated endocytosis (<100 nm).[28] The average particle size of RGD (−) and RGD (+) micelles was around 110 nm, with a moderate size distribution (polydispersity index = 0.14−0.18). Thus, these micelles are likely to be internalized by both clathrin- and caveolae-mediated endocytosis. Also, cyclic RGD peptides selectively recognize both $\alpha_v\beta_3$ and $\alpha_v\beta_5$ integrin receptors. $\alpha_v\beta_5$ integrins, which adenoviruses use for their internalization into target cells, are known to facilitate clathrin-mediated endocytosis,[29] while $\alpha_v\beta_3$ integrin-mediated internalization occurs via caveolae-mediated endosytosis.[30,31] Since $\alpha_v\beta_3$ integrins have 10-times higher binding affinity to cyclic RGD peptides than $\alpha_v\beta_5$ integrins,[32] it is reasonable to assume that RGD (+) micelles might preferably recognize $\alpha_v\beta_3$ integrins and thus to induce the caveolae-mediated endocytosis as the internalization route into HeLa cells. Alternatively, RGD (−) micelles, based on their size, might be primarily internalized by clathrin-mediated endocytosis and subsequently delivered to the acidic compartment of a lysosome. Caveolae-mediated endocytosis is not associated with a pH decrease, and is

(26) Fisher, K. D.; Ulbrich, K.; Subr, V.; Ward, C. M.; Mautner, V.; Blankey, D.; Seymour, L. W. A Versatile System for Receptor-Mediated Gene Delivery Permits Increased Entry of DNA into Target Cells, Enhanced Delivery to the Nucleus and Elevated Rates of Transgene Expression. *Gene Ther.* **2000**, *7*, 1337–1343.

(27) Hashimoto, M.; Morimoto, M.; Saimoto, H.; Shigemasa, Y.; Sato, T. Lactosylated Chitosan for DNA Delivery into Hepatocytes: The Effect of Lactosylation on the Physicochemical Properties and Intracellular Trafficking of pDNA/Chitosan Complexes. *Bioconjugate Chem.* **2006**, *17*, 309–316.

(28) Grosse, S.; Aron, Y.; Thevenot, G.; Francois, D.; Monsigny, M.; Fajac, I. Potocytosis and Cellular Exit of Complexes as Cellular Pathways for Gene Delivery by Polycations. *J. Gene Med.* **2005**, *7*, 1275–1286.

(29) Wickman, T. J.; Filardo, E. J.; Cheresh, D. A.; Nemerow, G. R. Integrin $\alpha_v\beta_5$ Selectively Promotes Adenovirus Mediated Cell Membrane Permeabilization. *J. Cell Biol.* **1994**, *127*, 257–264.

(30) Wary, K. K.; Mainiero, F.; Isakoff, S. J.; Marcantonio, E. E.; Giancotti, F. G. The Adaptor Protein Shc Couples a Class of Integrins to the Control of Cell Cycle Progression. *Cell* **1996**, *87*, 733–743.

(31) Wary, K. K.; Mariotti, A.; Zurzolo, C.; Giancotti, F. G. A Requirement for Caveolin-1 and Associated Kinase Fyn in Integrin Signaling and Anchorage-Dependent Cell Growth. *Cell* **1998**, *94*, 625–634.

(32) Marinelli, L.; Gottschalk, K.-E.; Meyer, A.; Novellino, E.; Kessler, H. Human Integrin $\alpha_v\beta_5$: Homology Modeling and Ligand Binding. *J. Med. Chem.* **2004**, *47*, 4166–4177.

known to be a nondigestive route of external substances into the cellular compartment.[33] Some nonenveloped viruses, such as simian virus 40, utilize this route for transfection to host cells and accumulate in a smooth endoplasmic reticulum compartment.[34,35] Thus, RGD (+) micelles internalized by caveolae-mediated endocytosis may be able to avoid pDNA degradation in acidic organelles, leading to high transfection efficiency. Moreover, as seen in the real-time luciferase assay under the "13 h mitosis" condition (Figure 7C), the luciferase expression of RGD (+) micelles detected at 30 h was remarkably higher than that of RGD (−) micelles, despite the comparable levels of cellular uptake between the two (Figures 3C and 4). Obviously, this result cannot be explained by the difference in the migration rate, because there was sufficient time for both RGD (+) and RGD (−) micelles to accumulate in the perinuclear region before mitosis. The higher gene expression of RGD (+) micelles is consistent with their preferential localization in caveosomes due to distinctive intracellular trafficking through the nonacidic and nondegradable route of caveolae-mediated endocytosis.

It should be noted that the results in Figures 5 and 6 indicate that not all of the RGD (+) micelles were internalized by caveolae-mediated endocytosis. Clathrin-mediated endocytosis, a relatively slow uptake pathway, could also contribute to the internalization of a portion of RGD (+) micelles, possibly due to the nonspecific interaction between the micelle and the cell membrane, even though polyplex micelles are covered with PEG to minimize nonspecific interaction. Nevertheless, the $\zeta$-potentials of the polyplex micelles still take small positive values, suggesting that PEG charge shielding is incomplete. This slight positive charge might induce the nonspecific interaction of polyplex micelles with the negatively charged cell membrane. If this is the case, an increase in the PEG density of polyplex micelles may reduce the interaction, increasing the ligand's effects on the uptake and gene expression of polyplex micelles. An alternative explanation on the nonspecific uptake of polyplex micelles is available by considering the amphiphilic character of the PEG molecule. A PEG chain under concentrated conditions, as found in the shell layer in the micelle system, might have the ability to interact with the plasma membrane components through hydrophobic interaction or indirectly through a bridge of hydrated water molecules.[36] Research to clarify the underlying mechanism is now under way in our laboratory, and the results will be reported elsewhere in the near future.

## Conclusions

In conclusion, polyplex micelles with integrated implementations of cyclic RGD peptide ligands on the micelle surface and disulfide cross-linking in the core achieved remarkably enhanced transfection efficiency against HeLa cells expressing $\alpha_v\beta_3$ integrins on the surface. The RGD ligands were effective not for increasing uptake but for modulating intracellular trafficking of polyplex micelles. RGD (+) micelles were distributed in the perinuclear region at an early period and were preferentially internalized by caveolae-mediated endocytosis via nonacidic and nondegradable intracellular compartments. These results indicate that polyplex micelles with cyclic RGD ligands and disulfide cross-links are promising approaches to facilitate cell-specific transfection by controlling intracellular trafficking as well as by the environment-sensitive release of encapsulated pDNA in the target cells.

Cyclic RGD peptide is well-known to selectively recognize $\alpha_v\beta_3$ integrin receptors identified as a marker of angiogenic vascular tissue,[37] and thus is a good candidate as a ligand for gene vectors used for diseases including tumor characterized by neovascularization. Indeed, nonviral gene vectors, in which cyclic RGD peptide ligands are installed have been applied to delivery pDNA and siRNA to tumor vasculature, effectively suppressing tumor growth.[13,14] Thus, polyplex micelle with cyclic RGD ligands and disulfide cross-links may be a useful system for cancer gene therapy through a systemic administration.

**Acknowledgment.** This work was financially supported in part by the Core Research Program for Evolutional Science and Technology (CREST) from Japan Science and Technology Corporation (JST), by Special Coordination Funds for Promoting Science and Technology (SCF) commissioned by the Ministry of Education, Culture, Sports, Science, and Technology (MEXT) of Japan, and by Grant-in-Aid for Nanomedicine Research from the Ministry of Health, Labour and Welfare (MHLW), Japan.

MP800070S

(33) Pelkmans, L.; Kartenbeck, J.; Helenius, A. Caveolar Endocytosis of Simian Virus 40 Reveals a New Two-Step Vesicular-Transport Pathway to the ER. *Nat. Cell Biol.* **2001**, *3*, 473–483.

(34) Norkin, L. C.; erson, H. A.; Wolfrom, S. A.; Oppenheim, A. Caveolar Endocytosis of Simian Virus 40 Is Followed by Brefeldin A-Sensitive Transport to the Endoplasmic Reticulum, Where the Virus Disassembles. *J. Virol.* **2002**, *76*, 5156–5166.

(35) Conner, S. D.; Schmid, S. L. Regulated Portals of Entry into the Cell. *Nature* **2003**, *422*, 37–44.

(36) Kataoka, K.; Kwon, G. S.; Yokoyama, M.; Okano, T.; Sakurai, Y. Block Copolymer Micelles as Vehicles for Drug Delivery. *J. Controlled Release* **1993**, *24*, 119–132.

(37) Brooks, P. C.; Clark, R. A.; Cherish, D. A. Requirement of Vascular Integrin $\alpha_v\beta_3$ for Angiogenesis. *Science* **1994**, *264*, 569–571.

*Pharmaceutical Research, Vol. 25, No. 12, December 2008 (© 2008)*
DOI: 10.1007/s11095-008-9720-2

*Research Paper*

# Polyplex Micelles from Triblock Copolymers Composed of Tandemly Aligned Segments with Biocompatible, Endosomal Escaping, and DNA-Condensing Functions for Systemic Gene Delivery to Pancreatic Tumor Tissue

**Kanjiro Miyata,[1,6] Makoto Oba,[2] Mitsunobu R. Kano,[3,6] Shigeto Fukushima,[4] Yelena Vachutinsky,[1] Muri Han,[5] Hiroyuki Koyama,[2] Kohei Miyazono,[3,6] Nobuhiro Nishiyama,[4,6] and Kazunori Kataoka[1,4,5,6,7]**

*Received June 26, 2008; accepted August 26, 2008; published online September 10, 2008*

***Purpose.*** For systemic gene delivery to pancreatic tumor tissues, we prepared a three-layered polyplex micelle equipped with biocompatibility, efficient endosomal escape, and pDNA condensation functions from three components tandemly aligned; poly(ethylene glycol) (PEG), a poly(aspartamide) derivative with a 1,2-diaminoethane moiety (PAsp(DET)), and poly(L-lysine).

***Materials and Methods.*** The size and *in vitro* transfection efficacy of the polyplex micelles were determined by dynamic light scattering (DLS) and luciferase assay, respectively. The systemic gene delivery with the polyplex micelles was evaluated from enhanced green fluorescence protein (EGFP) expression in the tumor tissues.

***Results.*** The polyplex micelles were approximately 80 nm in size and had one order of magnitude higher *in vitro* transfection efficacy than that of a diblock copolymer as a control. With the aid of transforming growth factor (TGF)-β type I receptor (TβR-1) inhibitor, which enhances accumulation of macromolecular drugs in tumor tissues, the polyplex micelle from the triblock copolymer showed significant EGFP expression in the pancreatic tumor (BxPC3) tissues, mainly in the stromal regions including the vascular endothelial cells and fibroblasts.

***Conclusion.*** The three-layered polyplex micelles were confirmed to be an effective gene delivery system to subcutaneously implanted pancreatic tumor tissues through systemic administration.

**KEY WORDS:** gene delivery; PEG; polyplex micelle; TGF-β inhibitor; triblock copolymer.

## INTRODUCTION

Successful gene delivery through systemic administration is crucial for the gene therapy of various intractable diseases, including cancer. Use of an appropriate gene vector is needed for systemic administration to achieve selective accumulation of the intact gene in target tissues, and subsequently, to reveal effective gene expression with a sufficient therapeutic index. Although major gene vectors in clinical trials are viral-based systems (1), they could have risks of immunogenicity and mutagenicity that would interfere with their practical use in clinics. Synthetic polymer-based vectors (polyplexes) are attractive alternatives of viruses, because of much lower immunogenicity, greater ease of chemical modification and larger-scale preparation (2–4). To attain successful transfection in tumor tissues *via* intravenous administration by polyplex vectors, several important issues as follows should be addressed: (1) high stability to protect the DNA structure in the biological milieu from nuclease attack, (2) minimized non-specific interaction with biological components to exert longevity in the blood circulation, and (3) smooth escape from endosomes to cytoplasm for efficient gene expression inside target cells.

To fulfill such requirements, polyplexes with poly(ethylene glycol) (PEG) palisades (polyplex micelle) have been prepared by several groups including ourselves through the self-assembly of PEG-polycation copolymers with plasmid DNA (pDNA) (4–8). Indeed, polyplex micelles prepared from PEG–poly(L-lysine) block copolymer (PEG–PLys) showed high tolerability in serum media (9), allowing for a prolonged circulation period of intact pDNA in the blood stream, whereas naked pDNA was completely digested within

[1] Department of Bioengineering, Graduate School of Engineering, The University of Tokyo, 7-3-1 Hongo, Bunkyo-ku, Tokyo, 113-8656, Japan.
[2] Department of Clinical Vascular Regeneration, Graduate School of Medicine, The University of Tokyo, 7-3-1 Hongo, Bunkyo-ku, Tokyo, 113-8655, Japan.
[3] Department of Molecular Pathology, Graduate School of Medicine, The University of Tokyo, 7-3-1 Hongo, Bunkyo-ku, Tokyo, 113-8655, Japan.
[4] The Center for Disease Biology and Integrative Medicine, Graduate School of Medicine, The University of Tokyo, 7-3-1 Hongo, Bunkyo-ku, Tokyo, 113-0033, Japan.
[5] Department of Materials Engineering, Graduate School of Engineering, 7-3-1 Hongo, Bunkyo-ku, Tokyo, 113-8656, Japan.
[6] Center for NanoBio Integration, The University of Tokyo, 7-3-1 Hongo, Bunkyo-ku, Tokyo, 113-8656, Japan.
[7] To whom correspondence should be addressed. (e-mail: kataoka@bmw.t.u-tokyo.ac.jp)

5 min (10). Nevertheless, PLys-based systems have encountered the issue of inefficient transfection activity, because of the lack of endosome escape, involving a "proton sponge effect" caused by amino groups with a low pKa value as typically reported in poly(ethylenimine) (PEI)-based systems (11,12). Worth noting in this regard is our recent finding that polyplexes from a poly(aspartamide) derivative having 1,2-diaminoethane unit as a side chain, poly[*N*-[*N*-(2-aminoethyl)-2-aminoethyl]aspartamide] (PAsp(DET)), revealed highly efficient transfection with minimal cytotoxicity to a variety of cells including primary cells (13–16), probably due to facilitated endosomal escape based on remarkable change in the protonation degree between physiological pH and endosomal acidic pH. Actually, the PEG–PAsp(DET) polyplex micelle succeeded in *in vivo* transfection of a reporter gene (luciferase) to a rabbit's clamped carotid artery *via* intra-arterial injection (17). Also, when the PEG–PAsp(DET) polyplex micelle was incorporated into a calcium phosphate cement scaffold and then applied in a bone defect model to a mouse skull bone, substantial bone formation surrounding the entire lower surface of the implant was induced by the regulated release of the micelles containing a constitutively active form of activin receptor-like kinase 6 (caALK6) and runt-related transcription factor 2 (Runx2) genes from the scaffold (18). The relatively weak affinity of PAsp(DET) segments to pDNA (19) is also an advantage for the smooth release of the incorporated pDNA and subsequent efficient transcription in the cell interior. On the other hand, such weak affinity probably leads to the detachment of PAsp (DET) chains from pDNA in the polyplex micelle through the interaction with biological components during circulation in the blood stream, resulting in a loss of transfection activity. Therefore, strategies to stabilize the structure of the polyplex micelles against PEG–PAsp(DET) are needed for the development of effective systemic administration methods.

The present study was devoted to develop a PEG–PAsp (DET)-based polyplex micelle for systemic use by conjugating a PLys segment as an anchoring moiety to pDNA at the ω-end of the diblock copolymer. For this purpose, a triblock copolymer of poly(ethylene glycol)-poly[*N*-[*N*-(2-aminoethyl)-2-aminoethyl]aspartamide]-poly(L-lysine) (PEG–PAsp (DET)–PLys) was prepared to integrate three functional segments engendering biocompatibility (PEG), efficient endosomal escape (PAsp(DET)), and effective pDNA condensation (PLys), respectively. In this way, three-layered polyplex micelles can be constructed, in which the middle layer, functioning as an endosomal escape element, is sandwiched between an outer layer of biocompatible PEG and an inner layer of PLys/pDNA polyplex (20). The fluorescence measurement with an intercalator into DNA indicated that pDNA mixed with the triblock copolymers was condensed more tightly than in a PEG–PAsp(DET) diblock copolymer and comparably to a PEG–PLys diblock copolymer. Intracellular trafficking of the polyplex micelles with or without the intermediate layer of PAsp(DET) was compared in detail by confocal fluorescence microscopy to reveal the endosomal escape of the micelles with the PAsp(DET) layer. Finally, reporter gene expression in a subcutaneous pancreatic tumor model, representing an intractable solid tumor with thick fibrosis and hypovascularity, demonstrated that the intravenously injected three-layered polyplex micelles effectively penetrated tumor vasculature in combination with transforming growth factor (TGF)-β type I receptor inhibitor (TβR-I) (21).

## MATERIALS AND METHODS

### Materials

α-Methoxy-ω-amino-poly(ethylene glycol) (Mw 12,000; PEG–$NH_2$) and β-benzyl-L-aspartate *N*-carboxy-anhydride (BLA–NCA) were obtained from Nippon Oil and Fats Co., Ltd. (Tokyo, Japan). ε-(Benzyloxycarbonyl)-L-lysine *N*-carboxy anhydride (Lys(Z))–NCA was synthesized from ε-(benzyloxycarbonyl)-L-lysine (Wako Pure Chemical Industries, Ltd., Osaka, Japan) by the Fuchs-Farthing method using bis(trichloromethyl) carbonate (triphosgene; Tokyo Kasei Kogyo Co., Ltd., Tokyo, Japan) (22). Diethylenetriamine (DET; bis(2-aminoethyl)amine), *N*,*N*-dimethylformamide (DMF), dichloromethane, benzene, trifluoroacetic acid, *N*-methyl 2-pyrrolidone (NMP), Tris (tris(hydroxymethyl) aminomethane) and HEPES (2-[4-(2-hydroxyethyl)-1-piperazinyl]ethanesulfonic acid) were purchased from Wako Pure Chemical Industries, Ltd., Osaka, Japan. DMF and dichloromethane distilled by conventional methods were used for the polymer synthesis. DET was distilled over $CaH_2$ under reduced pressure, and then used for the aminolysis reaction. A pDNA coding for luciferase with a CAG promoter provided by RIKEN (Japan) was used after the amplification in competent DH5α *Escherichia coli* and the subsequent purification using a HiSpeed Plasmid MaxiKit purchased from QIAGEN Science Co., Inc. (Germantown, MD, USA). A full-size Label IT Cy5 Labeling Kit was purchased from Mirus Bio Corporation (Madison, WI, USA). Twenty-four- and 96-well culture plates were purchased from Becton Dickinson Labware (Franklin Lakes, NJ, USA). A human hepatocyte, Huh-7, was obtained from the RIKEN Cell Bank (RIKEN Bioresource Center, Japan). A human pancreatic adenocarcinoma cell line, BxPC3, was obtained from the American Type Culture Collection (Manassas, VA, USA). Dulbecco's Modified Eagle's Medium (DMEM) and RPMI medium 1640 were purchased from Sigma-Aldrich Co. (St. Louis, MO, USA). Fetal bovine serum (FBS) was purchased from Dainippon Sumitomo Parma Co., Ltd. (Osaka, Japan). A Luciferase Assay System Kit was purchased from Promega Co. (Madison, WI, USA), and a Micro BCA™ Protein Assay Reagent Kit was purchased from Pierce Co., Inc. (Rockford, IL, USA). TβR-I inhibitor was purchased from Calbiochem (San Diego, CA, USA; LY364947; catalog no. 616451). Rat monoclonal antibody anti-platelet endothelial cell adhesion molecule-1 (PECAM-1), as a marker for vascular endothelial cells, was purchased from BD Pharmingen (Franklin Lakes, NJ, USA), and Alexa647-conjugated secondary antibody to rat IgG was from Invitrogen Molecular Probes (Eugene, OR, USA).

### Synthesis of PEG–PBLA–PLys(Z) Triblock Copolymer

A triblock copolymer, PEG–PBLA–PLys(Z), was synthesized as previously described (20). Briefly, the PEG–poly (β-benzyl L-aspartate) diblock copolymer (PEG–PBLA) was synthesized by the ring-opening polymerization of BLA–NCA initiated by PEG–$NH_2$, followed by the additional ring-

opening polymerization of Lys(Z)–NCA to obtain PEG–PBLA–PLys(Z) (Fig. 1). Different solvents were used for the syntheses of PEG–PBLA with varying degree of polymerization (DP). For example, PEG–PBLA (DP of PBLA=14) was prepared as follows: BLA–NCA (25 eq to the terminal primary amino group of PEG–$NH_2$) in DMF was added to PEG–$NH_2$ in DMF under an argon atmosphere, and stirred at 35°C for 20 h. After confirming the end of the polymerization from the disappearance of specific peaks of NCA in the IR spectrum (IR Report-100 spectrometer (JASCO, Tokyo, Japan)), the solution was poured into a mixture of *n*-hexane and ethyl acetate (6:4) to precipitate PEG–PBLA, and the precipitate was filtered and dried *in vacuo*. A series of PEG–PBLA with longer PBLA segments was prepared by a similar protocol with necessary changes in reaction conditions, including molar feed ratios of PEG–$NH_2$ to BLA–NCA, solvents and reaction times, as summarized in Table I. The obtained PEG–PBLAs were subsequently used for the ring-opening polymerization of Lys(Z)–NCA. Lys(Z)–NCA (50 eq to terminal primary amino group of PEG–PBLA) in a mixture of DMF and dichloromethane was added to PEG–PBLA in dichloromethane (final molar ratio of DMF to dichloromethane=1:10) under an argon atmosphere, and stirred at 35°C for 40 h. After confirming the end of the polymerization as in the case of the polymerization of BLA–NCA, the solution was poured into the 6:4 mixture of *n*-hexane and ethyl acetate to precipitate PEG–PBLA–PLys (Z), and the precipitate was filtered and dried *in vacuo*. Then, acetylation of the amino group of the N-terminal of PEG–PBLA–PLys(Z) was performed using acetic anhydride (3 eq to the terminal amino group of PEG–PBLA–PLys(Z)) in dichloromethane solution.

For estimation of the DP and molecular weight distribution (Mw/Mn) of the obtained PEG–PBLA–PLys(Z), a gel permeation chromatography (GPC) measurement was carried out using a TOSOH HLC-8220 equipped with TSKgel columns (Super AW4000 and Super AW3000X2), and an internal refractive index (RI) detector. NMP with 50 mM LiBr was used as an eluent at a flow rate of 0.3 ml $min^{-1}$ at 40°C.

### Preparation of PEG–PAsp(DET)–PLys Triblock Copolymer

Introduction of 1,2-diaminoethane units into the side chain of the PBLA segment in PEG–PBLA–PLys(Z) was performed by aminolysis reaction with excess of DET molecules (13), followed by the deprotection of the Z group with HBr/AcOH (Fig. 1). The typical synthetic procedure of PEG–PAsp(DET)–PLys with DP of PAsp(DET)=36 and PLys=50 was as follows: Three hundred milligram of PEG–PBLA–PLys(Z) (9.2 μmol) was lyophilized from benzene

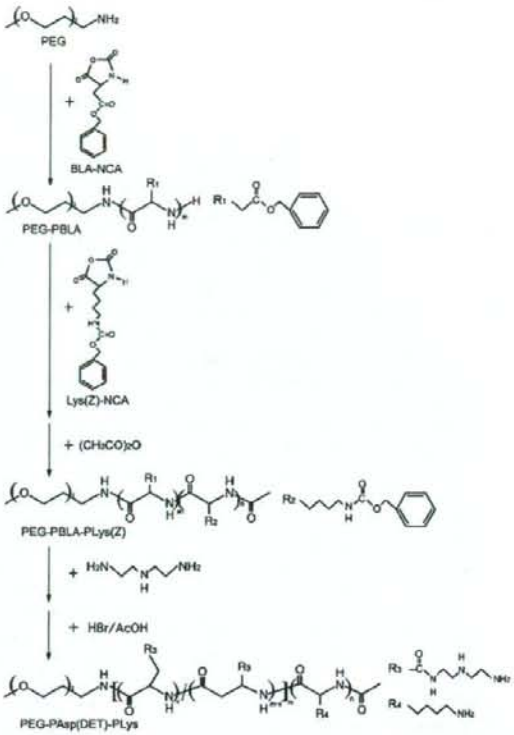


**Fig. 1.** Synthetic procedure of triblock copolymer, PEG–PAsp (DET)–PLys.

solution and dissolved into 6 mL of DMF. DET (1.8 mL, 16.7 mmol, 50 eq to benzyl groups of PBLA) was added under an argon atmosphere, and stirred at 40°C for 24 h. The mixture was dropped into diethyl ether (80 mL) with stirring, and then the white precipitate was filtered and redissolved in trifluoroacetic acid (2 mL). To deprotect the Z group, HBr (30% in acetic acid) was then added and stirred for 1 h, after which the solution was dropped into diethyl ether (40 mL) with stirring, and the resulting precipitate was purified by filtration and dried *in vacuo*. The crude product was dissolved in distilled water, dialyzed against 0.01 N HCl and then distilled water, and lyophilized to obtain the final product, PEG–PAsp(DET)–PLys as a hydrochloride salt form. The introduction of 1,2-diaminoethane units into the side chain of PAsp and the deprotection of Z group from the PLys(Z) segment were confirmed by $^1H$ NMR measurement ($D_2O$,

**Table I.** Reaction Condition and Composition of PEG–PBLA–PLys(Z)

| Code | Molar feed ratio (PEG:BLA:Lys(Z)) | Solvent/reaction time (h) for BLA polymerization | Solvent/reaction time (h) for Lys(Z) polymerization | DP of PBLA–PLys (Z)[a] | Mw/Mn[b] |
|---|---|---|---|---|---|
| PAsp14(DET)Lys48 | 1:25:50 | DMF/20 | DMF+$CH_2Cl_2$ (1:10)/40 | 14–48 | 1.16 |
| PAsp36(DET)Lys50 | 1:45:50 | DMSO/40 | DMF+$CH_2Cl_2$ (1: 10)/40 | 36–50 | 1.13 |
| PAsp66(DET)Lys47 | 1:80:50 | DMF + $CH_2Cl_2$ (1:10)/40 | DMF + $CH_2Cl_2$ (1:10)/40 | 66–47 | 1.28 |

[a] Determined from $^1H$ NMR.
[b] Determined from GPC.

80°C). In addition, other triblock copolymers, PEG-*b*-poly[*N*-(3-morpholylpropyl)aspartamide]-*b*-PLys (PEG–PAsp(APM)–PLys) and PEG-*b*-poly[*N*-(5-aminopentyl)aspartamide]-*b*-PLys (PEG–PAsp(DAP)–PLys), were similarly prepared by the aminolysis reaction of PEG–PBLA–PLys(Z) with 4-(3-aminopropyl)morpholine (20) and 1,5-diaminopentane (23), respectively. An $^1$H NMR spectrum was measured with a JEOL EX300 spectrometer (JEOL, Tokyo, Japan). Chemical shifts are reported in ppm downfield from 3-(trimethylsilyl) propionic acid-$d_4$ sodium salt.

### Cytotoxicity of PEG–PAsp(DET)–PLys Triblock Copolymer

A quantitative colorimetric assay with Cell Counting Kit-8 (Dojindo, Kumamoto, Japan) was carried out to evaluate cytotoxicity of block copolymers. This kit utilizes a colorimetric change from a soluble tetrazolium salt (WST-8) to WST-8 formazan by cytosolic dehydrogenases. Huh-7 cells (5,000 cells) were plated on 96-well plates and incubated overnight in 100 μL of DMEM containing 10% FBS. Then, the medium was changed to 100 μL of fresh medium containing 10% FBS and the polymers with various concentrations. After 24 h incubation, the medium was replaced with 100 μL of medium containing 10% FBS without polymers, followed by additional 24 h incubation. The medium was replaced with 120 μL of medium containing 10% FBS and 20 μL of Cell Counting Kit-8 solution, and then, incubated at 37°C for 3 h. The absorbance at 450 nm of the produced WST-8 formazan in each well was measured using a microplate reader (Model 680, Bio-rad). The cytotoxicity of block copolymers was estimated as a growth inhibitory concentration required for 50% reduction in cell population (IC50). The IC50 value of each block copolymer was calculated from a ratio of the obtained absorbance with the polymer to control without polymers. The results are presented as means and standard errors obtained from eight samples.

### Preparation of PEG–PAsp(DET)–PLys/pDNA Polyplex Micelle

Each polymer was dissolved in 10 mM Tris–HCl (pH 7.4) buffer at a concentration of 2–5 mg/mL. These polymer solutions were then mixed with pDNA solution in 10 mM Tris–HCl (pH 7.4; final pDNA concentration: 33 μg/mL for *in vitro* assay and 100 μg/mL for *in vivo* assay) at varying mixing ratios.

### Ethidium Bromide Exclusion Assay

Each polyplex micelle solution with 33 μg pDNA/mL, prepared by simply mixing pDNA and block copolymers at varying mixing ratios in 10 mM Tris–HCl (pH 7.4), was diluted to 10 μg pDNA/mL containing 2.5 μg EtBr/mL and 150 mM NaCl with the same buffer. The fluorescence intensity of the polyplex micelle solutions at $\lambda$=590 nm excited by UV laser (365 nm) was measured using a NanoDrop (ND-3300 Fluorospectrometer, Wilmington, DE, USA). The reference was set with 10 mM Tris–HCl (pH 7.4). The relative fluorescence intensity was calculated as follows:

$$F_r = (F_{sample} - F_0)/(F_{100} - F_0)$$

where $F_{sample}$ is the fluorescence intensity of the micelle samples, $F_{100}$ is that of the free pDNA, and $F_0$ is the background without pDNA. The results are presented as a mean and standard deviations (SD) obtained from three samples.

### Dynamic Light Scattering and Zeta Potential Measurements

DLS and zeta potential measurements were performed using a Zetasizer nanoseries (Malvern Instruments Ltd., UK) at a detection angle of 173° and a temperature of 37°C. An He–Ne laser ($\lambda$=633 nm) was used as an incident beam. Polyplex solutions with various $N^+$/P ratios were prepared to a pDNA concentration of 33 μg/mL in 10 mM Tris–HCl (pH 7.4) buffer. The $N^+$/P ratio was defined as the molar ratio of protonated amino groups in block copolymers at pH 7.4 to phosphate groups in pDNA. The protonation degrees of lysine and Asp(DET) units at pH 7.4 were estimated to be 1.0 and 0.5, respectively, from the potentiometric titration results (13,24). In the DLS measurement, the sample solutions were injected into a small glass cuvette (volume: 12 μL), ZEN2112 (Malvern Instruments, Ltd.). The data obtained from the rate of decay in the photon correlation function were analyzed by the cumulant method, and the corresponding hydrodynamic diameter of the micelles was then calculated by the Stokes–Einstein equation (25). In the case of zeta potential measurement, the sample solutions were injected into folded capillary cells (Malvern Instruments, Ltd.). From the obtained electrophoretic mobility, the zeta potential was calculated by the Smoluchowski equation:

$$\zeta = 4\pi\eta\upsilon/\varepsilon$$

where $\eta$ is the viscosity of the solvent, $\upsilon$ is the electrophoretic mobility, and $\varepsilon$ is the dielectric constant of the solvent. The results are presented as a mean and SD obtained from three samples.

### *In Vitro* Transfection (Luciferase Assay)

Huh-7 cells (20,000 cells) on 24-well culture plates were incubated with polyplex micelles containing 1 μg pDNA (Lys/Phosphate=2) in 400 μL of DMEM containing 10% FBS, followed by 24-h incubation and replacement with fresh medium. At 24 h post-incubation, the cells were washed with 400 μL of Dulbecco's PBS, and lysed with 200 μL of the cell culture lysis buffer (Promega). The luciferase activity of the lysates was evaluated from the photoluminescence intensity using the Luciferase Assay System and a Mithras LB 940 (Berthold Technologies). The obtained luciferase activity was normalized with the amount of proteins in the lysates determined by the Micro BCA™ Protein Assay Reagent Kit. The results are presented as means and standard errors obtained from four samples.

### Cellular Uptake Study of Polyplex Micelles

pDNA was radioactively labeled with $^{32}$P-dCTP using the Nick Translation System (Invitrogen, San Diego, CA, USA). Unincorporated nucleotides were removed using High Pure PCR Product Purification Kit (Roche Laboratories, Nutley, NJ, USA). After purification, 2 μg of labeled pDNA

was mixed with 400 μg of non-labeled pDNA. The polyplex micelle samples were prepared by mixing the radioactive pDNA solution with each polymer solution (Lys/Phosphate= 2 and 33 μg pDNA/mL). Huh-7 cells were seeded on 24-well culture plates in DMEM containing 10% FBS. After 24-h incubation, the cells were incubated for 24 h with 30 μL of the radioactive micelle solution (1 μg pDNA/well) in 400 μL of DMEM containing 10% FBS. The cells were then washed three times with Dulbecco's PBS and lysed with 400 μL of the cell culture lysis buffer. The lysates were mixed with 5 mL of scintillation cocktail, Ultima Gold (PerkinElmer, MA, USA), and the radioactivity of the mixtures was measured by a scintillation counter. The results are presented as means and standard errors obtained from four samples.

### Intracellular Distribution of Cy5-labeled pDNA Evaluated Through Confocal Laser Scanning Microscope

pDNA was labeled with Cy5 using the Label IT Cy5 Labeling Kit according to the manufacturer's protocol. Huh-7 cells (50,000 cells) were seeded on a 35-mm glass base dish (Iwaki, Japan) and incubated overnight in 1 mL DMEM containing 10% FBS. After replacement of used medium with 1 mL of fresh medium, 90 μL of polyplex solution (Lys/Phosphate=2) containing 3 μg of Cy5-labeled pDNA was applied to the glass dish. After 24-h incubation, the medium was removed and the cells were washed three times with PBS. The intracellular distribution of each polyplex was observed by CLSM after staining acidic late endosomes and lysosomes with LysoTracker Green (Molecular Probes, Eugene, OR, USA) and nuclei with Hoechst 33342 (Dojindo Laboratories, Kumamoto, Japan). The CLSM observation was performed using LSM 510 (Carl Zeiss, Germany) with a ×63 objective lens (C-Apochromat, Carl Zeiss, Germany) at the excitation wavelengths of 488 nm (Ar laser), 633 nm (He–Ne laser), and 710 nm (MaiTai laser for 2-photon imaging) for LysoTracker Green (green), Cy5 (red), and Hoechst 33342 (blue), respectively.

### *In Vivo* Enhanced Green Fluorescence Protein Expression in Subcutaneous Tumor Through Intravenous Injection of Polyplex Micelles

Human pancreatic adenocarcinoma cells (BxPC3) were grown in RPMI medium 1640 supplemented with 10% FBS. BALB/c nude mice (female, 5 weeks old) were obtained from Charles River Laboratories (Tokyo, Japan). All animal experimental protocols were performed in accordance with the Guide for the Care and Use of Laboratory Animals as stated by the NIH. BxPC3 cells ($5\times10^6$ cells in 100 μL of PBS) were injected subcutaneously into the BALB/c nude mice and allowed to grow for 2–3 weeks to reach the proliferative phase. TβR-I inhibitor, dissolved to 5 mg/mL in DMSO and diluted by 100 μL of PBS, was intraperitoneally injected at 1 mg/kg 24 h before polyplex micelle administration. Polyplex micelles (Lys/Phosphate=2) containing EGFP gene in 200 μL of 10 mM HEPES buffer (pH 7.4) were intravenously injected through the tail vein at a dose of 20 μg pDNA/mouse. The mice were sacrificed 3 days after the injection. Tumors were excised, fixed with 10% formalin, and frozen in dry-iced acetone. The frozen samples were further sectioned at a 10-μm thickness in a cryostat. Immunostaining was carried out using anti-PECAM-1 antibody followed by Alexa647-conjugated secondary antibody for staining of vascular endothelial cells. The samples were observed by LSM 510 at excitation wavelengths of 488 and 633 nm for EGFP (green) and Alexa647 (red), respectively.

## RESULTS

### Preparation of PEG–PAsp(DET)–PLys Triblock Copolymer

A triblock copolymer of PEG, PBLA, and PLys(Z) (PEG–PBLA–PLys(Z)) as a precursor of the cationic triblock copolymer, PEG–PAsp(DET)–PLys, was synthesized by the two-step ring-opening polymerization of BLA–NCA (step 1) and Lys(Z)–NCA (step 2), initiated from the primary amine of PEG–$NH_2$ as shown in Fig. 1. In this way, a series of triblock copolymers with varying DPs of PBLA and PLys(Z) segments were prepared. As summarized in Table I, the obtained PEG–PBLA–PLys(Z)s were confirmed to have narrow Mw/Mn from the GPC, and the number of repeating units in PBLA and PLys(Z) segments was calculated from the peak intensity ratio of PBLA and PLys(Z) to PEG in the $^1$H NMR spectra (data not shown). The conversion of flanking benzyl ester in the PBLA segment to *N*-(2-aminoethyl)-2-aminoethyl group was carried out by aminolysis reaction of PEG–PBLA–PLys(Z) with DET, followed by deprotection of the Z group of the PLys(Z) segment to obtain PEG–PAsp (DET)–PLys. The quantitative conversion of PBLA to PAsp (DET) and the complete deprotection of Z group were verified by $^1$H NMR from the peak intensity ratio of the methylene protons in the *N*-(2-aminoethyl)-2-aminoethyl group ($H_2N(CH_2)_2NH(CH_2)_2NH$–, $\delta$=3.1–3.5 ppm) to the β-methylene protons in the poly(aspartamide) (–$CHCH_2CO$–, $\delta$=2.8 ppm) and the disappearance of the Z group peaks ($C_6H_5CH_2$–, $\delta$=7.3 and 5 ppm), respectively, as typically seen in Fig. 2. The obtained PEG–PAsp(DET)–PLys was abbreviated as PAspX(DET)LysY, where X and Y represent the DP of the PAsp(DET) and PLys segments, respectively. Similarly, control diblock copolymers, PEG–PAsp(DET) and PEG–PLys, were abbreviated as PAspX(DET) and PLysY, respectively.

### Cytotoxicity of PEG–PAsp(DET)–PLys Triblock Copolymer

The cytotoxicity of block copolymers, PEG–PAsp(DET), PEG–PLys, and PEG–PAsp(DET)–PLys, was compared and summarized as IC50 values in Table II. Obviously, PEG–PAsp(DET) showed much lower cytotoxicity than the others. The IC50 value of PAsp36(DET)Lys50 at the basis of polymer concentration (μM) was the similar level to that of PLys48, indicating that introduction of PAsp(DET) intermediate segment between PEG and PLys has negligible influence on the cytotoxicity of the block copolymer.

### Formation of PEG–PAsp(DET)–PLys/pDNA Polyplex Micelles

Complex formation of pDNA with the triblock copolymer (PAsp36(DET)Lys50) was confirmed by EtBr exclusion assay. While EtBr molecules are known to emit strong fluorescence with their intercalation to DNA duplexes,

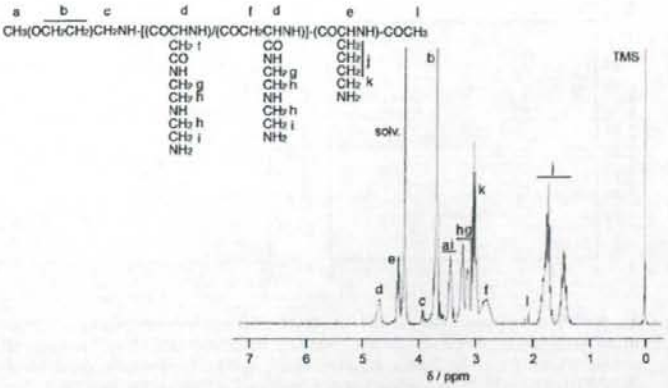


**Fig. 2.** $^1$H NMR spectrum of the triblock copolymer, PAsp36(DET)Lys50. (Solvent, $D_2O$; temperature, 80°C; concentration, 10 mg/mL).

DNA condensation by cationic molecules inhibits such intercalation, resulting in decreased fluorescence. Accordingly, the measurement of the EtBr fluorescence allows the estimation of the process of pDNA condensation (26). The obtained fluorescence data are shown in Fig. 3a. The N/P ratio was defined as the residual molar ratio of total amino groups in the block copolymer to phosphate groups in the pDNA. The fluorescence change in PAsp36(DET)Lys50 seems to reach a plateau at an N/P ratio of 1.5. On the other hand, PLys48 and PAsp39(DET) as control diblock polycations reached plateaus at different N/P ratios; i.e., 1 for PLys48 and 2 for PAsp39(DET). In the plateau region, the fluorescence intensity was similar between PLys48 and PAsp36(DET)Lys50 possessing the PLys segment, while PAsp39(DET) showed higher fluorescence intensity than the others. This result suggests that the PLys segment may have higher ability of pDNA condensation than the PAsp(DET) segment to induce effective dye-exclusion. Then, the fluorescence data was replotted against the residual molar ratio of protonated amino groups to phosphate groups ($N^+/P$ ratio; Fig. 3b). The protonation degree of Lys and Asp(DET) units at pH 7.4 was defined as 1.0 and 0.5, respectively, which were determined from potentiometric titration results of PEG–PLys (24) and PEG–PAsp(DET) diblock copolymers (13). Interestingly, in Fig. 3b, fluorescence profiles of all the samples showed similar trends, leveling off around the $N^+/P$ ratio of 1, indicating that the protonated fraction of amino groups principally participates in the complexation with phosphate groups in the pDNA.

**Table II.** Growth Inhibitory Effects of the Block Copolymers Against Huh-7 Cells

| | IC50 | | |
|---|---|---|---|
| Sample | Polymer concentration (μg/mL) | Polymer concentration (μM) | Amine concentration (μM) |
| PAsp68(DET) | >225 | >7.35 | >1,000 |
| PLys48 | 26.1±1.4 | 1.2±0.1 | 57.0±3.1 |
| PAsp36(DET)Lys50 | 29.5±0.8 | 0.9±0.04 | 114.4±4.9 |

### Size and Zeta Potential of PEG–PAsp(DET)–PLys/pDNA Polyplex Micelles

The size and surface charge of gene vectors crucially affect their biological performance. Thus, these values of the polyplex micelles were determined by DLS and zeta potential measurements, respectively. As shown in Fig. 4a, the size of polyplex micelles gradually decreased with the $N^+/P$ ratio, converging to the range of 60–80 nm in the region of $N^+/P>2$. The polyplex micelles from the triblock copolymer (PAsp36(DET)Lys50) were slightly smaller in size than those from the diblock copolymers (PAsp39(DET) and PLys48). As seen in Fig. 4b, all of the polyplex micelles showed almost neutral zeta potential at the $N^+/P$ ratio of 1. Nevertheless, the micelles kept their initial size without any agglomeration even after overnight standing, as is consistent with the formation of a PEG palisade surrounding the polyplex core. Increasing the $N^+/P$ ratio from 1 caused an increase in the zeta potential to a positive value, presumably due to the adsorption of excess block copolymers to the polyplex micelles as previously observed for PEG–P[Lys-*random*-Asp(DET)] block copolymer systems (19). The most prominent increase in the zeta potential with $N^+/P$ was observed for the PAsp36(DET)PLys50 system, which may be explained by the decrease in PEG density of polyplex micelles due to the relative increase in the total length of cationic segments in the block copolymers; e.g., 39 for PAsp39(DET), 48 for PLys48, and 86 for PAsp36(DET)Lys50. Providing the micelles have the same compositional $N^+/P$ ratio at a given feeding $N^+/P$ ratio, the density of PEG should decrease with an increase in the length of the cationic segment. In this regard, the values of the zeta potential were compared between PAsp36(DET)Lys50 triblock micelles and PLys109 diblock (PEG–PLys) micelles having longer-length cationic PLys segments (Fig. 4c). Obviously, the PAsp36(DET)Lys50 micelles still had higher zeta potential than the PLys109 micelles. This finding indicates that the zeta potential of polyplex micelles in the region of excess block copolymers is not simply correlated to the length of the cationic segment, and that the difference in the chemical structure of cationic amino acid residues, in this case Lys and PAsp(DET), crucially affects the composition and structure of the polyplex micelles.

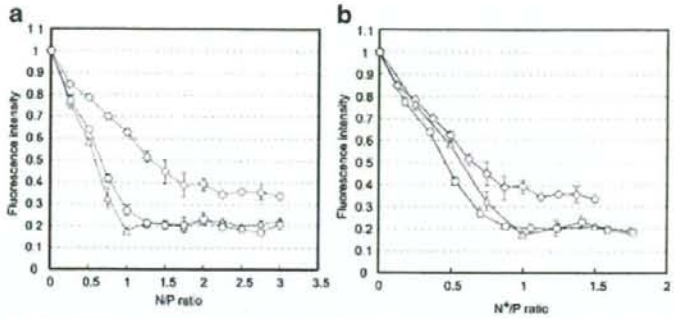


**Fig. 3.** EtBr dye exclusion assay on the polyplex micelles with varying compositions prepared from PAsp39(DET) (*diamonds*), PLys48 (*triangles*), and PAsp36(DET)Lys50 (*circles*; pDNA concentration, 10 μg/mL; EtBr concentration, 2.5 μg/mL; Temperature, 25°C; Medium, 10 mM Tris–HCl (pH 7.4) containing 150 mM NaCl). **a** The relationship with the N/P ratio, i.e., the residual molar ratio of amino groups in the polymer to phosphate groups in the pDNA. **b** The relationship with the $N^+/P$ ratio, the residual molar ratio of protonated amino groups in the polymer to phosphate groups in pDNA at pH 7.4. Results were expressed as mean±SD ($n$=3).

To verify the influence of the order of the cationic components in the triblock copolymer, the zeta potential of the polyplex micelles from PEG–PLys–PAsp(DET) (the DPs of PLys and PAsp(DET) were 48 and 33, respectively) was also measured. As seen in Fig. 4d, the polyplex micelles from PLys48Asp33(DET) showed the similar level of zeta potential to those from PLys48. This indicates that PAsp (DET) aligned as an intermediate segment contributes to the higher zeta potential of the PAsp36(DET)Lys50 (Fig. 4b–d).

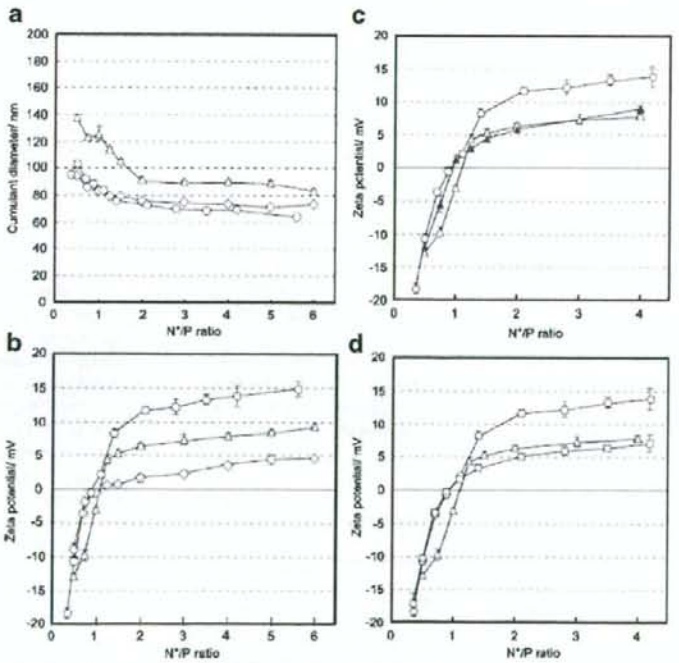


**Fig. 4.** Size and zeta potential of the polyplex micelles. **a** Size. **b**, **c**, **d** Zeta potential. PAsp39(DET); *diamonds*. PLys48; *empty triangles*. PLys109; *filled triangles*. PAsp36(DET) Lys50; *circles*. PLys48Asp33(DET); *squares*. (pDNA concentration, 33.3 μg/mL; Temperature, 37°C). Results were expressed as mean±SD ($n$=3).

### *In Vitro* Transfection with Polyplex Micelles Prepared from Triblock Copolymer with Varying Polycations as an Intermediate Segment

Polyplex micelles were prepared from triblock copolymers with different polycation segments aligned between PEG and PLys segments and were subjected to a luciferase assay against Huh-7 cells in order to explore whether the change in the chemical composition of the intermediate polycation layer affects the transfection efficiency. As will be addressed in "DISCUSSION" section, the polyplex micelles from triblock copolymer is likely to take three layered structure at least in the region of excess polycation ($N^+/P>1$): the outer layer of PEG, the middle layer of buffering polycation, and the inner core of condensed PLys/pDNA polyplex (20). PLys segment, which is almost fully charged at physiological pH, is assumed to principally participate in the polyplex formation, keeping the intermediate polycation as free form in the middle layer of the micelles. Thus, it may be reasonable to compare the transfection efficiency of these polyplex micelles from the triblock copolymers with different intermediate segments at the fixed Lys/Phosphate ratio instead of $N^+/P$ ratio, because the latter includes the contribution from the charged amino groups that may not directly participate in the polyplex formation. Here, the Lys/Phosphate ratio is fixed to 2 because the previous study revealed that pDNA condensation is completed at this ratio, exerting the optimal transfection efficiency (26).

The DPs of the intermediate polycations (PAsp(DAP), PAsp(APM), and PAsp(DET) as illustrated in Fig. 5a and the PLys in the triblock copolymers were fixed to 36 and 50, respectively, in this experiment. Fig. 5b clearly shows that the luciferase activity strongly depends on the structure of the intermediate polycation segments in the block copolymers. The polyplex micelles from the PAsp36(DAP)Lys50 showed a similar level of luciferase expression as those from the PLys48, indicating that the introduction of PAsp(DAP) segments with a similar pKa value, 9.9, to PLys had a negligible effect on the transfection efficacy. In line with our previous results (20), the polyplex micelles from the PAsp36(APM)Lys50 revealed some improvements in transfection efficacy compared to the PLys48 micelles. Notably, the highest transfection efficacy was achieved by polyplex micelles from the PAsp36(DET)Lys50, which showed tenfold higher luciferase activity than that from PLys48. On the other hand, the polyplex micelles from PEG–PLys–PAsp(DET) (the DPs of PLys and PAsp(DET) were 48 and 33, respectively), where the order of cationic segments between PAsp(DET) and PLys was inversed in the triblock copolymer, exhibited substantially decreased transfection efficacy compared with those from PAsp36(DET)Lys50.

The effect of the length of the cationic segments on the transfection efficacy was then studied in detail as seen in Fig. 5c. There was observed a critical increase in the transfection efficacy for PEG–PLys systems between the PLys20 and PLys48. It should be noted that one order of magnitude higher transfection was always obtained for the triblock systems compared to the diblock systems having similar total DPs of polycation segments (PLys71 *vs.* PAsp36(DET)Lys50 and PLys109 *vs.* PAsp66(DET)Lys47), supporting the result described in the preceding paragraph that the PAsp(DET) segment aligned as the intermediate segment plays a substantial role in the enhanced transfection.

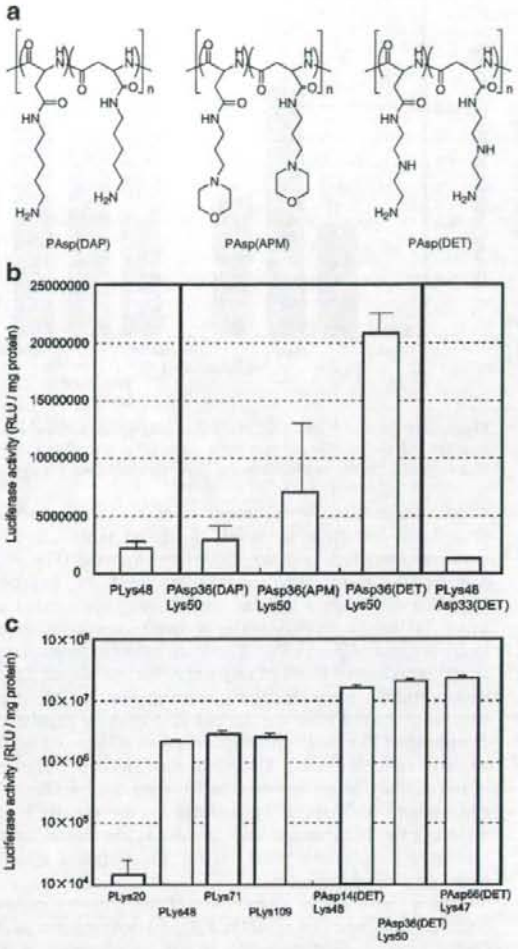


**Fig. 5.** Transfection efficacy of the polyplex micelles against Huh-7 cells (Luciferase assay). **a** Chemical structures of PAsp(DAP), PAsp (APM), and PAsp(DET) as the intermediate segment in the triblock copolymers. **b** Transfection efficacy of the polyplex micelles from PLys48, a series of triblock copolymers (PAsp36(R)Lys50) with varying intermediate segments (PEG–PAsp(DAP)–PLys, PEG–PAsp(APM)–PLys, and PEG–PAsp(DET)–PLys), and a triblock copolymer with the reversed order of the cationic segments, PLys48Asp33(DET). **c** Effect of the length of the cationic segments in di- or triblock copolymers on transfection efficacy. All the micelle samples were prepared at a Lys/Phosphate= 2 and applied for the transfection (pDNA concentration, 2.3 μg/mL).

### Cellular Uptake and Intracellular Distribution of PEG–PAsp (DET)–PLys/pDNA Polyplex Micelles

From the results of luciferase assay, a PAsp(DET) segment integrated into the middle of the triblock copolymers was confirmed to improve the transfection activity of the polyplex micelles, consistent with the hypothesis of facilitated

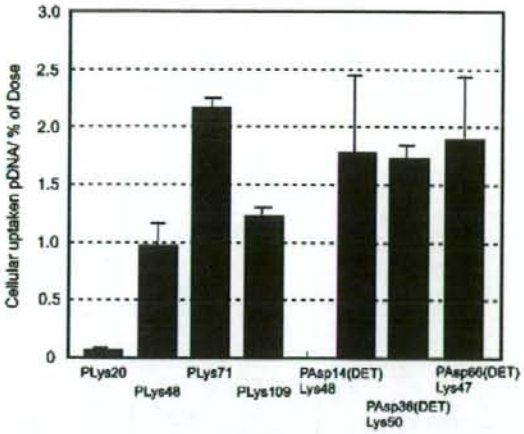


**Fig. 6.** Uptake into Huh-7 cells of $^{32}$P-labeled pDNA in the polyplex micelles. All the micelle samples were prepared at a Lys/Phosphate= 2 and applied for the experiments (pDNA concentration, 2.3 μg/mL).

endosomal escape. Nevertheless, there is also a possibility that the higher zeta potential of PEG–PAsp(DET)–PLys micelles compared to other PEGylated systems (Fig. 4b,c) may facilitate their cellular uptake, leading to the improved transfection. Hence, a cellular uptake study was carried out using $^{32}$P-labeled pDNA under a similar condition to the luciferase assay (Fig. 6). PLys20 micelle exhibited significantly lower uptake than those of other micelles, corresponding to its low transfection efficacy as shown in Fig. 5c. All of the micelles prepared from the diblock and triblock copolymers composed of PLys segments with DPs over 47 showed similar levels of cellular uptake. There was no significant difference in the efficacy of cellular uptake between the micelles with and without a PAsp(DET) segment as the middle block, excluding the facilitated cellular uptake as the reason for the improved transfection observed for the polyplex micelles from the triblock copolymers.

Then, intracellular distribution of the polyplex micelles from PLys48 and PAsp36(DET)Lys50 was observed by CLSM to estimate the efficacy of endosomal escape of the polyplex micelles. The pDNA, nuclei, and late endosomes/lysosomes were simultaneously stained with Cy5 (red), Hoechst33342 (blue), and LysoTracker (green), respectively. The Cy5-pDNA introduced into the PLys48 micelles without a PAsp(DET) segment was observed as discrete dots partially colocalizing with the late endosome/lysosome markers (yellow spots) 24 h after the addition of the polyplex micelles (Fig. 7a), indicating that the PLys48 polyplex micelles were segregated in intracellular compartments including late endosomes/lysosomes. In contrast, the Cy5-pDNA in PAsp36 (DET)Lys50 polyplex micelles spread more clearly in the cytoplasmic region (Fig. 7b), demonstrating that effective endosomal escape had occurred. These results strongly support that the PAsp(DET) segment plays a crucial role in facilitating the endosomal escape of the polyplex micelles.

### *In Vivo* Transfection by PEG–PAsp(DET)–PLys/pDNA Polyplex Micelle by Intravenous Administration

The transfection ability of the PAsp36(DET)Lys50 polyplex micelles by systemic administration was estimated from EGFP expression in subcutaneously xenografted human pancreatic adenocarcinoma, BxPC3. As previously reported, this tumor tissue has a poorly differentiated histology with a certain number of blood vessels and thick fibrotic tissue in the stroma (21); i.e., closely resembling the histology of certain intractable tumors observed in clinical specimens. The fluorescence microscopy of the sectioned xenografted tumors was obtained with immunostaining of tumor vasculature by PECAM-1 (red), and nuclear counter staining (blue; Fig. 8a). Apparently, the BxPC3 tumors were shown to have wide stromal regions (region S) surrounding nests of tumor cells (region T) and blood vasculature (region V). Fig. 8b shows the image of EGFP expression (green) in the BxPC3 tumor tissue receiving intravenous injection of the PAsp36(DET) Lys50 polyplex micelles incorporating pDNA coding for EGFP. The EGFP expression was evident, yet the intensity was very weak. Worth noting is that TβR-I inhibitor, which has been found to facilitate the accumulation of macromolecular drugs in tumor tissues (21), drastically improved the EGFP expression by the PAsp36(DET)Lys50 polyplex micelles (Fig. 8c). Note that the PAsp36(DET)Lys50 polyplex

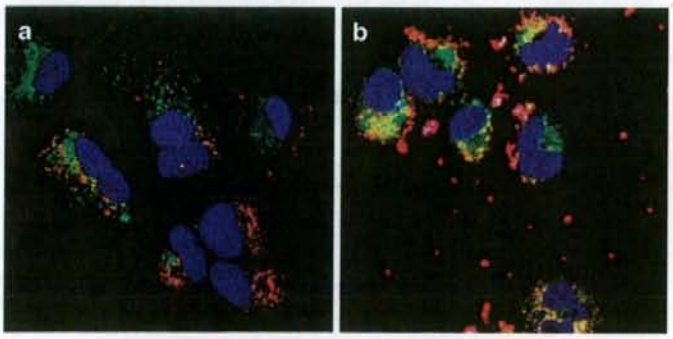


**Fig. 7.** Intracellular distribution of the PLys48 (**a**) and PAsp36(DET)Lys50 (**b**) micelles prepared at a Lys/Phosphate=2. The pDNA was labeled with Cy5 (*red*), and the late endosomes/lysosomes and the nucleus were stained with LysoTracker (*green*) and Hoechst33342 (*blue*), respectively. (pDNA concentration, 2.8 μg/mL).

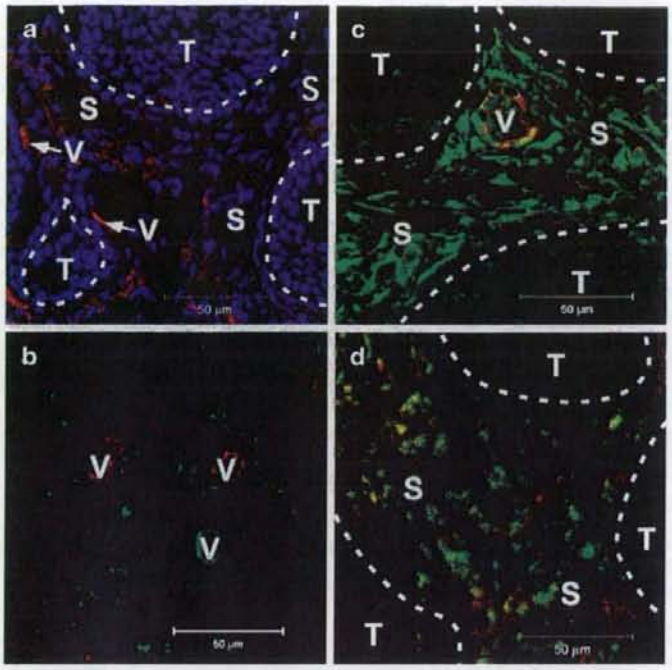


**Fig. 8.** EGFP transfection into subcutaneous tumors of pancreatic adenocarcinoma cells, BxPC3, *via* systemic route. Each micelle sample was prepared at a Lys/Phosphate=2, and intravenously injected through the tail veins of the mice (20 μg pDNA/mouse). **a** Histology of BxPC3 xenograft as a model of poorly differentiated pancreatic tumor tissue. *Blue*: nucleus stained with Hoechst 33342, *red*: PECAM-1 as an endothelial marker stained with Alexa647-conjugated secondary antibody against anti-PECAM-1 antibody (regions *T*, *S*, and *V* indicate nests of tumor cells in tumor tissues, thick fibrotic tissue in the stroma, and blood vasculature, respectively). **b** EGFP expression by PAsp36(DET)Lys50 polyplex micelle without TβR-I inhibitor; **c** EGFP expression by PAsp36(DET)Lys50 polyplex micelle with TβR-I inhibitor; **d** EGFP expression by PLys71 polyplex micelles with TβR-I inhibitor.

micelles in combination with TβR-I inhibitor did not show detectable EGFP expression in the liver and lung under the tested conditions (data not shown). Fig. 8d shows the result obtained for the PLys71 polyplex micelles with TβR-I inhibitor. Obviously, the EGFP expression by the PAsp36 (DET)Lys50 polyplex micelles was much more remarkable than that with the PLys71 polyplex micelles, suggesting that the integration of the PAsp(DET) segment into the polyplex micelles is effective even in the transfection by systemic administration. Detailed observation of the fluorescence images revealed that the EGFP expression by the polyplex micelles was located mainly around PECAM-1-positive vascular endothelial cells. As typically shown in Fig. 8a, the tumor stroma grows around the nests of tumor cells in BxPC3 subcutaneous xenografts, and blood vasculature exists inside the stroma. Therefore, a major part of the EGFP expression in the BxPC3 tumor by PAsp36(DET)Lys50 polyplex micelles was not from BxPC3 cells *per se*, but from cells in the stroma including vascular endothelial cells and fibroblasts.

## DISCUSSION

In the present study, polyplex micelles with an endosomal escape layer were prepared from a triblock copolymer for the purpose of transfection into solid tumors through systemic routes. The triblock copolymer was composed of three tandemly aligned functional segments as follows: PEG for biocompatibility, PAsp(DET) for efficient endosomal escape, and PLys for pDNA condensation. A series of triblock copolymers, PEG–PAsp(DET)–PLys, with the DP of PLys of approximately 50, was synthesized and used for the preparation of the polyplex micelles, according to the previous results that a DP of approximately 48 was needed for effective transfection with polyplex micelles from PEG–PLys as shown in Fig. 5c as well as for the prolonged circulation of intact pDNA in the blood stream (10). The triblock copolymer, PAsp36(DET)Lys50, as well as the diblock PEG–PLys, PLys48, effectively condensed pDNA to form a polyplex micelle (Fig. 3). The obtained polyplex micelles

from the triblock copolymer were around 80 nm at an $N^+/P$ ratio of 1 or greater (Fig. 4a), thereby having the potential ability to accumulate in tumors through the enhanced permeability and retention (EPR) effect (27). Also, the zeta potential measurement indicated that the excess positive charge of the polyplex micelle from the triblock copolymer was reasonably shielded by a PEG palisade surrounding the polyplex core (Fig. 4b). It should be noted that PEGylation of polyplexes facilitates their penetration into tumor spheroids (15, 16). Hence, the PEG palisade of polyplex micelles from the triblock copolymer may contribute to promoting their permeation into the tumor tissue *via* extravasation as well as to extending their plasma half-life through a steric stabilization effect, leading to appreciable gene expression in the subcutaneous pancreatic tumor tissue as seen in Fig. 8. Note that the xenografted pancreatic tumor, BxPC3, was chosen as our target in this study. Since pancreatic tumors are representative of intractable tumors, which are difficult to treat by conventional therapy, they are an appropriate target for the development of new strategies including gene therapy. However, it is also difficult to deliver exogenous genes to such tumor tissue by gene carriers through an EPR effect, presumably due to their thick fibrotic and hypovascular characteristics. In this regard, the combined use of TβR-I inhibitor, which has been found to decrease pericyte coverage of the endothelium specifically in tumor neovasculature (21), is available for the enhancement of accumulation of nano-carriers of 60–100 nm diameter into the solid tumor. Indeed, the EGFP expression by the polyplex micelles from PAsp36 (DET)Lys50 was substantially improved by the intraperitoneal injection of TβR-I inhibitor (Fig. 8b,c). The size of the polyplex micelle was approximately 80 nm, thereby making it suitable for combination with TβR-I inhibitor. As far as we know, this is the first example of effective gene expression in BxPC3 tumors with thick fibrotic and hypovascular characteristics *via* systemic administration of non-viral vectors. In addition, detailed observation of the fluorescence images from sectioned xenografted tumors revealed that the EGFP expression by the PAsp36(DET)Lys50 polyplex micelle combined with TβR-I inhibitor was located mainly around the blood vasculature (Fig. 8c), suggesting that the transfection with the polyplex micelle was not effective for the tumor cells *per se*, but for the cells in the tumor stroma, including vascular endothelial cells and fibroblasts. These results suggest that the penetration of polyplex micelles into tumor microenvironments may still be a major challenge, even with the aid of TβR-I inhibitor for successful systemic transfection directly to the BxPC3 tumor cells. In this regard, for the gene therapy of pancreatic adenocarcinoma with thick fibrotic tissues, the approach of treating the tissues surrounding the nests of tumor cells would be more realistic than that directly targeting tumor cells *per se*, e.g., with a tumor suppressor gene to induce apoptosis. Antiangiogenic gene therapy is one of the typical "indirect" approaches to treating fibrotic tumors, and research in this direction on combination treatment using polyplex micelles and TβR-I inhibitor is now ongoing in our laboratory.

The contribution of the PAsp(DET) segment in the triblock copolymer to improved transfection without increased cytotoxicity was obvious from the results of both *in vitro* and *in vivo* transfection studies (Figs. 5, 8, and Table II). It should be noted that there is no significant difference in cellular uptake between the polyplex micelles from the triblock and diblock copolymers (Fig. 6), even though the former revealed almost one order of magnitude higher transfection efficacy than the latter. This result suggests that the major cause for the facilitated transfection with the polyplex micelles from the triblock copolymer may be in the intracellular stage. Indeed, the CLSM observation clearly revealed the facilitated endosomal escape of pDNA associated with the polyplex micelles from the triblock copolymer (Fig. 7), indicating the availability of PAsp(DET) as an endosomal escape element. PAsp(DET) is likely to form the middle layer between the PEG shell and the PLys/pDNA polyplex core in the micelles, because PLys with higher affinity to pDNA than PAsp(DET) is assumed to undergo preferential condensation of pDNA, relegating the PAsp (DET) segment to the boundary with the PEG layer. Increased freedom of PLys as an outer block with a free chain-end may also contribute to the preferential complexation with pDNA. Note that a similar three-layered structure was previously proposed by us for polyplex micelles prepared from PEG–PAsp(APM)–PLys based on the results of $^1$H-NMR spectroscopy (20). The appreciably higher zeta potential of PAsp36(DET)Lys50 micelles in the region at an $N^+/P$ ratio of 1 or greater is consistent with the formation of a cationic middle layer (Fig. 4b,c) that is not completely shielded by the outer PEG layer. Thus, the PAsp(DET) placed in the middle layer of polyplex micelles should exert endosomal escape ability for efficient transfection through strong buffering and/or a membrane-destabilizing effect based on the unique two-step protonation behavior of the 1,2-diaminoethane unit (13,15). On the other hand, as seen in Fig. 5b, the one order of magnitude lower transfection efficacy obtained by reversing the order of PLys and PAsp (DET) segments in the triblock copolymer is interesting. It is reasonable to consider that arrangement of the PLys segment, with its strong condensing power against pDNA, as the intermediate segment of the triblock copolymer may allow the PAsp(DET) segment to become embedded in the core of the polyplex micelles, resulting in the loss of buffering and/or membrane-destabilizing capacity. The zeta potential of the PEG–PLys–PAsp(DET) systems similar to that of the PEG–PLys systems also supports the disappearance of the intermediate buffering layer in the polyplex micelles from PEG–PLys–PAsp(DET) with the reversed order of the cationic segments (Fig. 4d).

## CONCLUSION

For the achievement of systemic gene delivery to solid tumors with appreciable transfection efficacy, gene carriers are required to exert integrated functions including a stealth property in the blood stream to deliver intact pDNA into tumor tissues and permeate target cells with smooth translocation from endosomal compartments into the cytoplasm, subsequently releasing the pDNA to induce effective transcription. In the present study, to develop a gene carrier with such integrated functions, three segments with distinctive functions; i.e., PEG for biocompatibility, PAsp(DET) for endosomal escape, and PLys for pDNA condensation, were tandemly aligned in a polymer strand to form three-layered

polyplex micelles. The obtained micelles showed one order of magnitude higher transfection efficacy against Huh-7, compared to the micelles from the PEG–PLys diblock copolymer without any segments exerting an endosomal escape function. Notably, the polyplex micelle from the triblock copolymer achieved clear *in vivo* transfection of the EGFP gene in fibrotic pancreatic adenocarcinoma, BxPC3, through systemic administration. It should be emphasized that the EGFP expression in the pancreatic tumor was drastically enhanced by the intraperitoneal injection of TβR-I inhibitor prior to the micelle injection, and thus, the potential for combined therapy using polyplex micelles and TβR-I inhibitor for systemic transfection to solid tumors was clearly evidenced. Furthermore, detailed observation of the immunostained tumor tissues revealed that the EGFP expression by the triblock copolymer micelles was located mainly in the stromal tissues surrounding the nests of tumor cells. These results suggest that the triblock micelle is quite promising for fibrotic tumor treatments by the approach of transfecting the tissues surrounding tumor cells, including fibroblasts and endothelial cells, to express proteins inhibiting tumor angiogenesis.

## ACKNOWLEDGEMENTS

This work was financially supported by the Core Research Program for Evolutional Science and Technology (CREST) from the Japan Science and Technology Corporation (JST) as well as by Special Coordination Funds for Promoting Science and Technology from the Ministry of Education, Culture, Sports, Science and Technology of Japan (MEXT).

## REFERENCES

1. Wiley (2007) Gene Therapy Clinical Trials Worldwide, provided by the *J. Gene Med.* http://www.wiley.co.uk/genetherapy/clinical/ (accessed 17/01/08)
2. D. W. Pack, A. S. Hoffman, S. Pun, and P. S. Stayton. Design and development of polymers for gene delivery. *Nat. Rev. Drug Discov.* **4**:581–593 (2005) doi:10.1038/nrd1775.
3. E. Mastrobattista, M. A. E. M. van der Aa, W. E. Hennink, and D. J. A. Crommelin. Artificial viruses: a nanotechnological approach to gene delivery. *Nat. Rev. Drug Discov.* **5**:115–121 (2006) doi:10.1038/nrd1960.
4. E. Wagner. Strategies to improve DNA polyplexes for *in vivo* gene transfer: Will "artificial viruses" be the answer? *Pharm. Res.* **21**:8–14 (2004) doi:10.1023/B:PHAM.0000012146.04068.56.
5. Y. Kakizawa, and K. Kataoka. Block copolymer micelles for delivery of gene and related compounds. *Adv. Drug Deliv. Rev.* **54**:203–222 (2002) doi:10.1016/S0169-409X(02)00017-0.
6. S. Katayose, and K. Kataoka. Water-soluble polyion complex associates of DNA and poly(ethylene glycol)-poly(L-lysine) block copolymer. *Bioconjugate Chem.* **8**:702–707 (1997) doi:10.1021/bc9701306.
7. M. A. Wolfert, E. H. Schacht, V. Toncheva, K. Ulbrich, O. Nazarova, and L. W. Seymour. Characterization of vectors for gene therapy formed by self-assembly of DNA with synthetic block co-polymers. *Hum. Gene. Ther.* **10**:2123–2133 (1996) doi:10.1089/hum.1996.7.17-2123.
8. Y. H. Choi, F. Liu, J. Kim, Y. K. Choi, J. S. Park, and S. W. Kim. Polyethylene glycol-grafted poly-L-lysine as polymeric gene carrier. *J. Control. Release.* **54**:39–48 (1998) doi:10.1016/S0168-3659(97)00174-0.
9. K. Itaka, A. Harada, K. Nakamura, H. Kawaguchi, and K. Kataoka. Evaluation by fluorescence resonance energy transfer of the stability of nonviral gene delivery vectors under physiological conditions. *Biomacromolecules.* **3**:841–845 (2002) doi:10.1021/bm025527d.
10. M. Harada-Shiba, K. Yamauchi, A. Harada, I. Takamisawa, K. Shimokado, and K. Kataoka. Polyion complex micelles as a vector in gene therapy—pharmacokinetics and *in vivo* gene transfer. *Gene. Ther.* **9**:407–414 (2002) doi:10.1038/sj.gt.3301665.
11. O. Boussif, F. Lezoualc'h, M. A. Zanta, M. D. Mergny, D. Scherman, B. Demeneix, and J. Behr. A versatile vector for gene and oligonucleotide transfer into cells in culture and *in-vivo* polyethylenimine. *Proc. Natl. Acad. Sci. U. S. A.* **92**:7297–7301 (1995) doi:10.1073/pnas.92.16.7297.
12. M. Neu, D. Fischer, and T. Kissel. Recent advances in rational gene transfer vector design based on poly(ethylenimine) and its derivatives. *J. Gene Med.* **7**:992–1009 (2005) doi:10.1002/jgm.773.
13. N. Kanayama, S. Fukushima, N. Nishiyama, K. Itaka, W.-D. Jang, K. Miyata, Y. Yamasaki, U. Chung, and K. Kataoka. A PEG-based biocompatible block catiomer with high buffering capacity for the construction of polyplex micelles showing efficient gene transfer toward primary cells. *Chem. Med. Chem.* **1**:439–444 (2006) doi:10.1002/cmdc.200600008.
14. K. Masago, K. Itaka, N. Nishiyama, U. Chung, and K. Kataoka. Gene delivery with biocompatible cationic polymer: pharmacogenomic analysis on cell bioactivity. *Biomaterials.* **28**:5169–5175 (2007) doi:10.1016/j.biomaterials.2007.07.019.
15. M. Han, Y. Bae, N. Nishiyama, K. Miyata, M. Oba, and K. Kataoka. Transfection study using multicellular tumor spheroids for screening non-viral polymeric gene vectors with low cytotoxicity and high transfection efficiencies. *J. Control Release.* **121**:38–48 (2007a) doi:10.1016/j.jconrel.2007.05.012.
16. M. Han, Y. Bae, N. Nishiyama, and K. Kataoka. Gene delivery with poly(amino acid)-based block catiomer polyplex micelles against multicellular tumor spheroid. *Abstracts of 13th International Symposium on Recent Advances in Drug Delivery Systems*, Salt Lake City, UT, (2007b), pp. 128.
17. D. Akagi, M. Oba, H. Koyama, N. Nishiyama, S. Fukushima, T. Miyata, H. Nagawa, and K. Kataoka. Biocompatible micellar nanovectors achieve efficient gene transfer to vascular lesions without cytotoxicity and thrombus formation. *Gene. Ther.* **14**:1029–1038 (2007) doi:10.1038/sj.gt.3302945.
18. K. Itaka, S. Ohba, K. Miyata, H. Kawaguchi, K. Nakamura, T. Takato, U. Chung, and K. Kataoka. Bone regeneration by regulated *in vivo* gene transfer using biocompatible polyplex nanomicelles. *Mol. Ther.* **15**:1655–1662 (2007) doi:10.1038/sj.mt.6300218.
19. K. Miyata, S. Fukushima, N. Nishiyama, Y. Yamasaki, and K. Kataoka. PEG-based block catiomers possessing DNA anchoring and endosomal escaping functions to form polyplex micelles with improved stability and high transfection efficacy. *J. Control Release.* **122**:252–260 (2007) doi:10.1016/j.jconrel.2007.06.020.
20. S. Fukushima, K. Miyata, N. Nishiyama, N. Kanayama, Y. Yamasaki, and K. Kataoka. PEGylated polyplex micelles from triblock catiomers with spatially ordered layering of condensed pDNA and buffering units for enhanced intracellular gene delivery. *J. Am. Chem. Soc.* **127**:2810–2811 (2005) doi:10.1021/ja0440506.
21. M. R. Kano, Y. Bae, C. Iwata, Y. Morishita, M. Yashiro, M. Oka, T. Fujii, A. Komuro, K. Kiyono, M. Kamiishi, K. Hirakawa, Y. Ouchi, N. Nishiyama, K. Kataoka, and K. Miyazono. Improvement of cancer-targeting therapy, using nanocarriers for intractable solid tumors by inhibition of TGF-beta signaling. *Proc. Natl. Acad. Sci. U. S. A.* **104**:3460–3465 (2007) doi:10.1073/pnas.0611660104.
22. W. H. Daly, and D. Poche. The preparation of *N*-carboxyanhydrides of alpha-amino-acids using bis(trichloromethyl)carbonate. *Tetrahedron Lett.* **29**:5859–5862 (1988) doi:10.1016/S0040-4039(00)82209-1.
23. A. Koide, A. Kishimura, K. Osada, W. -D. Jang, Y. Yamasaki, and K. Kataoka. Semipermeable polymer vesicle (PICsome) self-assembled in aqueous medium from a pair of oppositely charged block copolymers: physiologically stable micro-/nanocontainers of water-soluble macromolecules. *J. Am. Chem. Soc.* **128**:5988–5989 (2006) doi:10.1021/ja057993r.
24. A. Harada, S. Cammas, and K. Kataoka. Stabilized α-helix structure of poly(L-lysine)-block-poly(ethylene glycol) in aque-